EMRTC Final Report #FR-9312

for NRL/DARPA Program

on

DYNAMIC HIGH-PRESSURE SHOCK COMPACTION OF DIAMOND POWDERS

(NRL Contract No: N00014-91-C-2173)

Submitted to

Dr. James E. Butler

Code 6170, Bldg. 207
4555 Overlook Avenue, S.W.
Naval Research Laboratory
Washington, D.C. 20375

by

EMRTC, New Mexico Tech,
Socorro, New Mexico 87801

May 25, 1993

The work reported here is done under NRL contract No. N00014-91-C-2173 to EMRTC, New Mexico Tech, with subcontracts to CalTech and Allied-Signal, Inc. The COTR at NRL is Dr. Jim Butler (Tel: 202-767-1115), and the Program Manager at DARPA is Dr. William J. Barker (Tel: 703-696-2281).

EMRTC/New Mexico Tech
N.N. Thadhani (505-835-5177)*
P.A. Persson (505-835-5818)
A. Grebe, V.S. Joshi (835-5595)

FAX: 505-835-5680

CALTECH
T.J. Ahrens (818-356-6906)
D. Goodwin (818-356-4249)
N.W. Page and H.-S. Shin

FAX: 818-564-0715

Allied-Signal, Morristown
Z. Iqbal (201-455-3899)
R. Baughman (455-3899)

FAX: 201-455-4807

*present address: School of Materials Science & Engineering, Georgia Tech, Atlanta, Tel: 404-894-2651)

REPORT DOCUMENTATION PAGE

Form Approved
OMB No. 0704-0188

1. AGENCY USE ONLY (Leave blank)	2. REPORT DATE	3. REPORT TYPE AND DATES COVERED
	25 May 1993	Final Report- May 1991-25May 1993

4. TITLE AND SUBTITLE

Dynamic High Pressure Shock Compaction of Diamond Powders

5. FUNDING NUMBERS

N00014-91-C-2173

6. AUTHOR(S)

N.N.Thadhani, P.A.Persson, A.Grebe, V.S.Joshi (EMRTC)
T.J.Arhens, D.Goodwin, N.W.Page, H.S.Shin (CALTECH)
Z.Iqbal, R.Baugman (Allied Signal)

7. PERFORMING ORGANIZATION NAME(S) AND ADDRESS(ES)

EMTRC, New Mexico Tech, Socorro, NM 87801
Califirnia Institute of Technology, Pasedena, CA 91125
Allied Signal Inc., Morristown, NJ 07960

8. PERFORMING ORGANIZATION REPORT NUMBER

EMRTC Final Report
FR-93-12

9. SPONSORING/MONITORING AGENCY NAME(S) AND ADDRESS(ES)

Dr. James E. Butler
Code 6170, Bldg. 207
4555 Overlook Ave., S.W.
Naval Research Laboratory
Washington, D.C. 20375

Program Manager (DARPA)
Dr. William J. Barker
1400 Wilson Blvd.
Arlington, VA 22209-2308

10. SPONSORING/MONITORING AGENCY REPORT NUMBER

11. SUPPLEMENTARY NOTES

12a. DISTRIBUTION/AVAILABILITY STATEMENT

Unlimited

12b. DISTRIBUTION CODE

13. ABSTRACT (Maximum 200 words)

The present report summarizes investigations carried out on shock consolidation of diamond powders for fabrication of compacts for electronic substrate applications. Consolidation of various types of commercially available natural and synthetic diamond powders has been performed in this study. The type of diamond and morphology of the powder particles affects the consolidation mechanisms as well as the diamond compact characteristics. It is shown that with the use of appropriate particle size distribution, and therefore a high initial packing density, compacts with optimum physical characteristics (crack-free and better than 90% of theoretical maximum density can be obtained. However, about 3-5% transformed graphite and extensive residual strain in the compacts has been detected, both of which severely limit the thermal conductivity. The work contained in this report provides an extensive series of experimental results and mechanistic studies discussing the consolidation behavior of diamond powders by the shock compression technique.

14. SUBJECT TERMS

Diamond, Shock Compaction, Powders

15. NUMBER OF PAGES

84

16. PRICE CODE

17. SECURITY CLASSIFICATION OF REPORT	18. SECURITY CLASSIFICATION OF THIS PAGE	19. SECURITY CLASSIFICATION OF ABSTRACT	20. LIMITATION OF ABSTRACT
UNCLASSIFIED	UNCLASSIFIED	UNCLASSIFIED	SAR

EXECUTIVE SUMMARY

The present report entitled "Dynamic High Pressure Shock Consolidation of Powders" summarizes results of collaborative investigations of researchers from New Mexico Tech, California Institute of Technology, and Allied-Signal, Inc., for fabrication of diamond compacts for electronic substrate applications. The fabrication process involved the use of dynamic processing techniques to consolidate commercially available diamond powders.

The objective of this work was to fabricate 1 mm thick diamond compacts by consolidation of powders by shock waves generated by impact of a projectile accelerated using explosive systems or propellant-gun launched techniques. The criterion for the consolidation of diamond powders of various types (natural and synthetic) and different particle sizes (<1 μm to >20 μm), treated with different types of surface cleansing and coating processes, was studied. The fundamental issues investigated in this work included establishing the effects of starting powder characteristics and shock consolidation conditions, as well as correlating these effects to the microstructure and other properties of the compacts.

Diamond compacts ~12 mm diameter by 1 mm thickness, made from various types of commercially available natural and synthetic powders were consolidated to densities in the range of 90-95% theoretical maximum density (TMD). Optimum consolidation conditions were achieved by appropriately controlling initial powder packing densities and compacting powders at shock conditions generated at impact velocities of 1.6 - 2.2 km/s.

Thermal conductivities of the diamond compacts were obtained indirectly via ultrasonic velocity measurements and also directly by a technique employing laser pulsed photothermal radiometry.

Ultrasonic measurements revealed a mean effective phonon velocity ~0.28 times that of single crystal diamond. Assuming a direct correlation between phonon velocity and thermal conductivity, it can be estimated that shock-processed diamond compacts have a thermal conductivity one-third of that of the single crystal. Direct measurements of thermal conductivity performed using the Laser Pulsed Photothermal Radiometry (PPR) technique yielded anomalously low values.

We attribute the low thermal conductivity of the shocked diamond compacts to be due to retention of 3-5% non-diamond (graphitic or amorphous carbon) phase, porosity, and residual strain due to the large defect concentration produced from extensive shock-induced plastic deformation. The thermal conductivity of the diamond compacts is also limited by that of the starting powders, and metallic and organic contaminations present in the starting diamond powders.

We believe that the type of diamond compacts produced by shock consolidation of powders in the present study are the first of their kind in terms of overall compact integrity and physical, mechanical, and microstructural characteristics. However, there are many issues that still remain unresolved. The time available in the present work has been too limited to allow detailed and in-depth diagnostics, calculations, observations and measurements. Without such evaluations and understanding, and specific process-microstructure-property correlations, the complete scope of the shock consolidation technique, may be difficult to infer for the fabrication of diamond substrates.

ABSTRACT

The present report summarizes investigations carried out on shock consolidation of diamond powders for fabrication of compacts for electronic substrate applications. Consolidation of various types of commercially available natural and synthetic diamond powders has been performed in this study. The type of diamond and morphology of the powder particles affects the consolidation mechanisms as well as the diamond compact characteristics. It is shown that with the use of appropriate particle size distribution, and therefore a high initial packing density, compacts with optimum physical characteristics (crack-free and better than 90% of theoretical maximum density can be obtained. However, about 3-5% transformed graphite and extensive residual strain in the compacts has been detected, both of which severely limit the thermal conductivity.

The work contained in this report provides an extensive series of experimental results and mechanistic studies discussing the consolidation behavior of diamond powders by the shock compression technique.

TABLE OF CONTENTS

CHAP. 1 - INTRODUCTION AND BACKGROUND

Amongst all other crystalline solids, diamond is the hardest material known, it has the highest thermal conductivity at room temperature, it is inert to all chemicals, and it is transparent to visible light, infrared, ultraviolet radiation and x-rays.[1] These properties make diamond attractive in applications ranging from superhard cutting tools and wear-resistant coatings for mechanical and optical components, to heat-sink substrates for electronic semi-conductor devices.[2]

High pressure and high temperature techniques used for synthesizing diamond from graphite have proved economical and yield a product of consistent quality and properties. However high pressure synthesis techniques have their limitations. These techniques result in diamond crystals no larger than 1-2 carats in size. Scale-up and impurity-free synthesis using a high-pressure diamond press is difficult and also expensive.

Thin diamond films can be used to coat large sized components by **"Chemical Vapor Deposition" (CVD)**,[3-6] employing either **plasma-assisted CVD (PACVD)** or **energetic ion-beam deposition (EIBD)**. The plasma-assisted CVD technique is much easier to implement and requires simple equipment assembly, and hence is more popular. Also, the hardware is relatively inexpensive and fairly high deposition rates can be accomplished. However, this technique requires high temperatures and relies on epitaxial film growth. Thus the range of substrate materials on which diamond films can be coated is somewhat limited. In contrast, techniques based on energetic ion beam deposition require much more complicated and costly hardware. The deposition rates are slower in this technique but processing temperatures are much lower and thus the process is not sensitive to substrate composition.

Chemical vapor deposition of diamond films proceeds by excitation of mixtures of hydrogen, hydrocarbon, and inert gases

either in a DC glow discharge or with RF or microwave radiation. In the process a plasma is produced, and carbon atoms are liberated by the thermal decomposition of the hydrocarbon gas. In order to ensure dissociation of the hydrocarbon gas and provide enough thermal energy to allow carbon to bond as diamond, the temperatures in the plasma discharge must exceed 800 to 1100°C. The free carbon atoms in the plasma have enough energy to permit tetragonal (diamond) bonding, however, upon condensation, the diamond films produced are not just tetragonally-bonded carbon (diamond), but may also contain mixtures of trigonally-bonded (graphite), and other allotropic crystalline forms of carbon.

1.1 Diamonds for Thermal Substrate Applications

With the multitude of today's advances in the semiconductor industry and its continued development, **thermal dissipation problems** have resulted in the inability of many electronic devices to operate at their premium capacity. Swan[7] in 1967, first reported that a greater heat conduction efficiency is possible with type IIa diamond heat sinks in contrast to copper and silver.

Diamond has a unique combination of very high thermal conductivity (highest of all materials at room temperature) and high electrical resistivity which can allow it to remove heat rapidly from high-power devices while maintaining electrical integrity. Single crystal wafers of diamond can thus be used as a substrate for certain high power laser diodes as well as for other electronic packaging systems. The cost of single-crystal diamond makes its widespread use uneconomical. Natural diamonds (particularly the nitrogen-free type IIa) are also used as thermal substrates (heat sinks), but their scarce availability and the dimensions in which they are available, limit their large-scale applications.

1.2 Dynamic shock consolidation of diamond powders

Shock consolidation of diamond powders is a unique and potentially highly efficient process. Consolidation of powders occurs due to localized deposition of shock energy (from collapse of voids) at particle surfaces, which results in interparticle fusion and bonding. Various mechanistic models have been proposed which describe the consolidation process. Three successively more sophisticated physical consolidation models will be described in the context of the present study.

(a) Simple Sliding Model and Regime: During the passage of a strong shock wave through an initially porous powder, the relatively high velocity of individual particles causes the grains to vigorously deform against, slide past one another, and fill in the porosity. After the shock-wave passage, this results in a virtually void-free solid containing heavily deformed particles, as shown in the micrograph and the simulations in Figure 1.

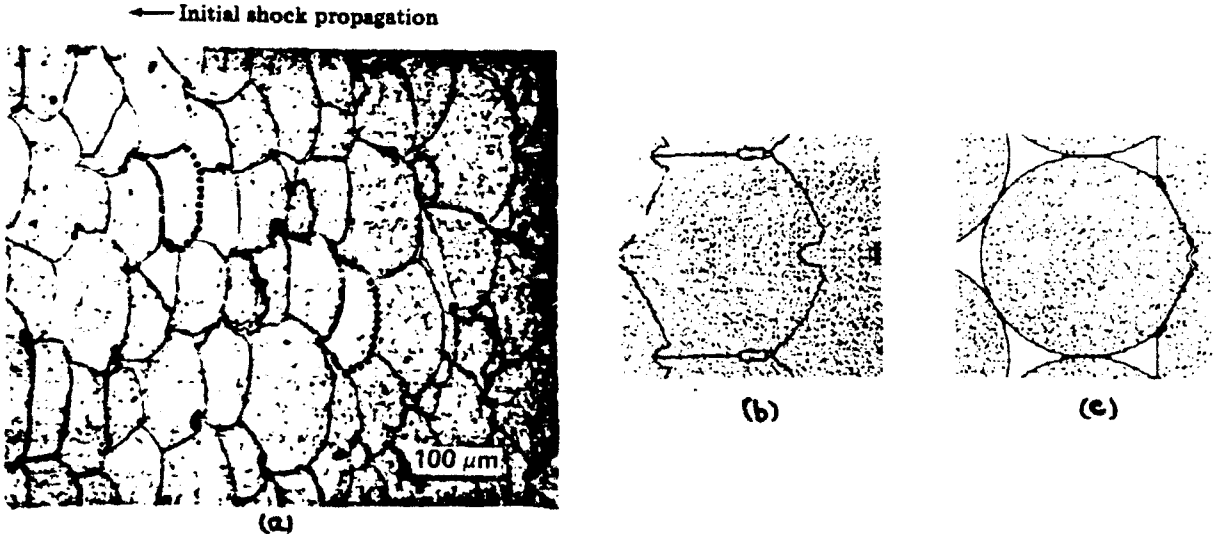

Fig. 1. Characteristic shape of shock consolidated, initially spherical powder. (a) Microphotograph of 37 μm diameter spheres compacted with 5.6 GPa shock wave propagating from right to left.[8] (b) and (c) computer simulation, 48 and 30 ns after 1km/s impact onto 10% porous rods.[9]

Previous experimental data has demonstrated that most of the shock energy goes into frictional sliding and plastic deformation at surfaces of, e.g. diamond grains, and that these become coated with a (carbon) melt. (At high dynamic pressures, diamond melts rather than vaporizing as it does at lower pressures). For consolidation to occur, the thermal content of the molten carbon layer on the particle surface must be transferred via both Fourier and radiative heat transfer into the interior of the diamond grain in time, t_f, before dynamic pressure is relieved. For the simplest model of shock consolidation then, the maximum mass fraction of melted material, L, is given by Ahrens et al[10]:

$$L = \frac{\frac{u_2}{2}}{[C_p(T_m - T_o) + \Delta H_m]} \qquad (1)$$

Equation (1) assumes that the kinetic energy (per unit mass) of particle motion (velocity, u) equals the internal energy deposited by the shock and all this energy goes into heating a mass fraction, L, which is at the surface layer of the powder grains. The thermal energy goes into raising the initial temperature, T_o, to the melt temperature T_m, and the associated enthalpy of melting is ΔH_m. Here, C_p is the specific heat. For particle velocities of $\sim 10^3$ m/sec, values of $L \approx 0.05$ are calculated for the properties of diamond. Particle velocities of $\sim 10^3$ m/sec in diamond powders with initial bulk density of ~2.0 g/cm^3 or 60% TMD (3.51 g/cm^3), are achieved using shock pressures of 20 GPa.

The duration of the shock pulse must exceed the time required to quench the molten layer surrounding each grain. Quenching or freezing time, t_f, is given by Potter and Ahrens as:[11]

$$t_f = \frac{\pi D}{16}\left(\frac{L\, d\Delta H_m}{DC_p(T_m - T_o)}\right)^2 \qquad (2)$$

where D is thermal diffusivity and d is mean grain diameter. For the thermal properties of diamond, assuming an 8 μm particle

diameter, the freezing time is very short (~10^{-8} s), compared to the typical durations of shock consolidation pressure pulses (10^{-6} to 10^{-5} s). Equation (2) allows prediction of the largest grain size which may be shock consolidated for a given duration pressure pulse, which for diamond with $t_f = 10^{-6}$ s, is ~10^2 μm.

(b) Homogeneous Heating Model: Samples consolidated, starting with material at room temperature within the sample sliding regime (as described by the physics outlined in (a)) suffer from excessive brittle rather than the desired ductile deformation. In laboratory experiments, two approaches have been utilized which allow plastic (dislocation generation and motion) deformation under shock loading conditions to occur. High temperature quasi-static deformation studies by Brookes et al.[12] demonstrate that dislocation generation can be associated with plastic deformation in diamond at pressures above 10 GPa at temperatures as low as 1300 K. Because of the marked incompressibility of diamond, this relatively modest temperature is, however, not easily achieved (except on grain boundaries) upon dynamic consolidation of the usual 60 to 70% of crystal density starting powders. Continuum temperatures, in which thermal equilibrium between the grain boundaries and the center of the powder grain are assumed, have been calculated and are shown in the carbon phase diagram in Figure 2 for graphite (m = 1) and for porous diamond for m = 1.43 and m = 1.92. Here m, the distension, is the ratio of the crystal density to powder density.

Continuum temperatures shown in Figure 2 are achieved when thermal equilibrium times, t_e ($\approx d^2/D$) are attained. For 10 μm diamond grain, $t_e = 10^{-6}$ sec. For very small crystallites, the shock transit time through the grain approaches t_e and consolidation of 0.1 μm diameter grains are predicted to be difficult. This is because although a thin film of molten material may form around these tiny grains, the excess heat of the film is both radiated and conducted into the interior of diamond particle so rapidly that consolidation between diamond grains cannot occur.

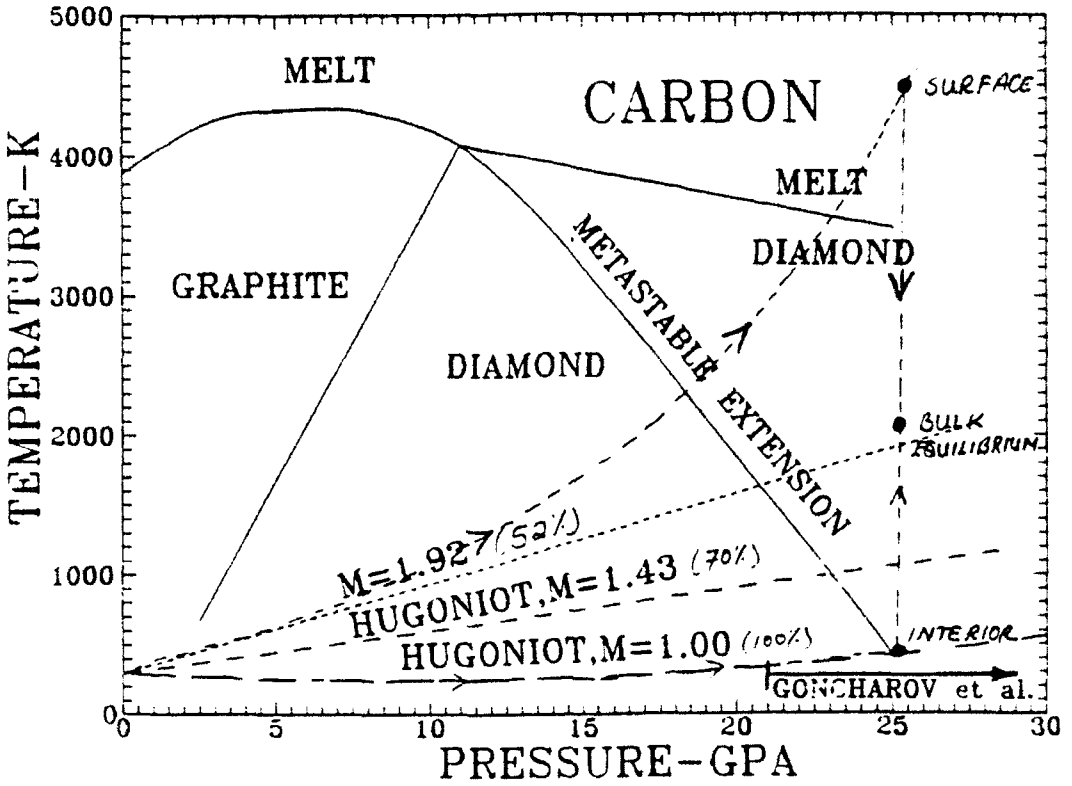

Fig. 2. Phase diagram of Carbon. Principle Hugoniot (m=1.00) intersection with metastable extension of graphite melt line is predicted to form carbon glass. Goncharov et al[13] demonstrated that graphite forms carbon glass upon static compression above 20 GPa. Porous diamond Hugoniots with distensions of 1.43 and 1.92 are shown.

However, for grains with diameters within the range of 1 to 10 μm and for distensions approaching m = 2 (e.g., m = 1.92 of Figure 4) shock temperatures approaching the regime of plastic (dislocation controlled) deformation is expected. Such plastic deformation of diamond has recently been reported upon shock consolidation of ~0.5 μm diamond powder by Kondo and Sawai.[14] Very recently, Hokamoto et al.[15] reported markedly well shock consolidated diamond powders were obtained upon preheating assemblies to relatively modest temperatures (900°K). Thus, by both starting with highly porous fine-grained powders and/or preheating powders, well consolidated, crack-free diamond compacts can be obtained via the dynamic method.

(c) Consolidation of Diamond Via Phase Transition: A third route to shock consolidation of diamond has been demonstrated by Potter and Ahrens[16]. They employed fine grained graphite as a coating on diamond powders prior to shock consolidation. Graphite is a low pressure phase of carbon with an initial crystal density of 2.26 g/cm^3, whereas the high pressure phase of carbon, diamond, has a crystal density of 3.51 g/cm^3. As demonstrated in Fig. 2, shock compression of graphite above 2.5 GPa, drives the graphite phase into the stability field of diamond. However, a large number of previous studies[16] of shock compression of graphite demonstrate that due to inhibition by kinetic effects, a factor of ten greater pressure is, in fact, required to shock-induce the graphite to diamond phase transition. Also, recently, Goncharov et al.[13] have demonstrated that above 20 GPa, graphite undergoes an intermediate transformation to a glassy phase (see Figure 4 also) prior to transformation to diamond. Thus, the effect of coating a fine layer of graphite onto diamond powder is observed to assist the consolidation by the formation of both fine grained diamond and a glassy phase which provides an interdiamond grain bonding agent.

1.3 Prior Work and Rationale

In this section, prior work on diamond powder compaction, that formed the basis of the current study will be briefly reported. Various attempts have been made to consolidate diamond powders by shock consolidation.[18] In recent years, the attempts by Potter and Ahrens,[11,16] Akashi and Sawaoka,[19,20] Yoshida et al.,[21] and Kondo and Sawai[14] have demonstrated successful compaction. Potter and Ahrens[16] used diamond powders of different particle sizes, and observed good consolidation but pronounced fracturing with 100-150 μm powders, minimum consolidation with ultrafine submicron powders, and strong well bonded (80-85% dense) compacts with 4-8 μm powders. Their results are essentially similar to those of Akashi and Sawaoka,[19,20] who also explained that the shock

consolidation mechanisms for diamond, include densification by particle fracture and solid-state bonding for coarse powders and by plastic deformation and solid-state fusion for fine powders.

Shock consolidation experiments performed by Kondo and Sawai[14] have been based on the mechanistic analysis applied to ultrafine powders. In this treatment consideration is given to spatial and temporal partitioning of shock-induced thermal energy, between skin (surface layer) and bulk particle. Thus, according to this treatment, the diamond powder particle dimensions need to be smaller than the heat dissipation time through the skin thickness. The experiments of Kondo and have yielded good compaction with densities in the 85-90% range, although the compacts have been extensively cracked and measurable levels of graphitization have been observed.

The extensive prior works on shock consolidation of difficult-to-bond ceramic and metallic powders have revealed that full densification can be achieved by the shock compression process along with complete retention of the characteristics of the starting materials. The rationale for the present work was therefore to advantageously utilize the beneficial properties of the high thermal conductivity type IIa natural diamond powders and/or the synthetically made high quality diamond powders. In addition, unlike other diamond substrate fabrication techniques that involve diamond growth rates of several microns per hour and have size and scaling limitations, the shock compaction technique is energy efficient, involves very quick processing times, and has virtually no size or scaling limitations.

1.4 Objectives, Program Plan, and Approach

The objectives of our program was to fabricate diamond compacts, to near solid density, by shock consolidation of powders. The emphasis of the study was focussed on establishing the consolidation criterion and optimum conditions of process variables and powder characteristics, that yield diamond compacts with high density as well as high thermal conductivity.

The approach adopted was to conduct consolidation experiments on different types of diamond powders (natural and synthetic) after subjecting them to various heat treatments and surface conditioning operations. The shock consolidation experiments were conducted at different shock-compression conditions, attained by impacting powders, packed at different initial green densities, at different velocities.

The recovered diamond compacts were characterized by density measurements and a variety of microstructural analysis tools including x-ray diffraction, scanning electron microscopy, Raman spectroscopy, and thermal/electrical conductivities. Finally, heat flow computations were made to correlate the consolidation characteristics based on degree of bonding and interparticle densification, and the various suggested consolidation mechanisms.

In the following chapters, we will provide a detailed description of the experimental approach, including the types and characteristics of starting diamond powders, the shock compaction technique and process variables, and compact characterization approach and technique. Details of the experimental results, highlighting the effects of different processing variables will be presented in Chapter 3, the microstructural characteristics in Chapter 4, and thermal conductivity measurements in Chapter 5. The compaction criterion and consolidation mechanisms relevant to diamond powders will be discussed Chapter 6, and a summary and concluding remarks will be provided in Chapter 7.

CHAP. 2 - EXPERIMENTAL TECHNIQUES

In order to develop an optimum shock processing scheme required for making 1 mm thick free-standing diamond substrates, a test matrix was established to study three classes of variables, including: shock processing environment, shock loading and unloading conditions, and choice of starting material characteristics. More specifically, the following variables were studied in the present program.

(a) Choice of Diamond Powder, Nature or Man-Made, Type I/II The thermal diffusivity of shock consolidated diamond from nature, man-made, Type I and Type II, and Type IIa enriched in $^{12}C^{42}$ may be widely different. Several of these powder types were used to determine which of a possible range of starting materials are most effective for shock consolidation.

(b) Initial Particle Size and Distribution - Successful shock consolidation has been conducted on diamond starting with grain sizes of 0.1 - 30 μm. Consolidation experiments to optimize particle size and distribution as a function of shock amplitude and duration were performed to generate information needed for full-scale processing.

(c) Porosity - Successful shock consolidation has also been conducted for diamond powders with 30 to 48% porosities. Thus, a series of systematic studies were conducted to delineate the range of initial porosities for optimum shock processing.

(d) Shock-Induced Thermal Annealing - Previous studies have demonstrated that by embedding diamond powders in between layers of powder mixtures which undergo shock-induced exothermic reactions, such as,

$$Fe_2O_3 + 2Al \rightarrow 2\ Fe + Al_2O_3 \quad (3)$$

$$Ti + C \rightarrow TiC \quad (4)$$

temperature rises of ~10^3K can be achieved. The heat in the mixture then propagates into the diamond compact during its

cooling from the consolidation temperature. Crack-free compacts have been made by this technique. A limited number of experiments were performed to explore the feasibility of this approach.

(e) Impedance Matching Media - In previous studies two approaches to obtaining shock consolidated crack-free free-standing plates of polycrystalline diamond have been researched. Surrounding the diamond powder in a non-bonding impedance matching media (e.g., porous Al_2O_3) appears, from the recent work of Mutz and Vreeland,[22] to be a promising method which can eliminate cracking upon stress wave unloading. In this case a single shock wave does the consolidation. Experiments to evaluate the suitability of Al_2O_3 as the enclosing media for shock consolidation were conducted in the present work. Another approach adopted was to employ plates of a refractory metal (e.g., tungsten) surrounding the diamond powder, in which case multiple reflected shocks consolidate the diamond.

(f) Shock Energetics - The optimum shock pressure, and hence, energy for compaction of different porosity media was explored. In particular, the attempts were focussed on establishing the narrow window within which sufficient energy localization only to heat and fuse diamond particles is available, without having the heat be retained for long enough times that can lead to formation of non-diamond phases.

2.1 Diamond Powders and Characteristics

Diamonds are generally classified,[1] according to their optical and electrical properties and their impurity contents, into four types of single crystal material and two types of polycrystalline natural diamond. Type Ia are by far the most abundant (~98%) type of natural diamond. These diamonds contain up to 0.1% nitrogen causing them to strongly absorb ultraviolet light. Nitrogen also induces infrared absorption and limits

thermal conductivity. **Type Ib** diamonds are typical of those produced by high pressure synthesis, but account for only 1% of natural diamonds. These contain up to 0.2% nitrogen incorporated in the lattice. Their optical, thermal, and electrical properties are similar to **type Ia** diamonds. **Type IIa and IIb** diamonds are both very rare. They are practically free of nitrogen, have the highest thermal conductivity and fairly low electrical resistivity, and are p-type semiconductors.

Carbonados and ballas are naturally occurring but extremely rare (0.2%) of all polycrystalline diamonds. **Carbonados** contain graphite and other impurities, but are much tougher than single-crystal diamonds, hence are generally used for abrasive applications. **Carbonados** can also be synthesized and sintered to make cutting tools. **Ballas** diamonds are round, dense and randomly oriented polycrystals, which do not cleave and are thus very impact resistant.

A variety of different types of commercially available natural and synthetic diamond powders were acquired in the present work. The selection of the starting diamond powders was based on: (i) properties relevant to substrate performance, (ii) properties desirable for shock compaction and (iii) cost and commercial availability of the powders. There exists very little information on thermal properties of the different types of commercially available natural and synthetic diamond powders, relevant to electronic substrate applications. The property of powders of important consideration relevant to shock consolidation is the particle morphology (shape, size, and surface characteristics). As is obvious from Section 1.2 and 1.3, the consolidation mechanisms and recovery of diamond compacts can be significantly affected by starting powder morphology. Powder morphology also affects the green density, and therefore the shock consolidation conditions. The various types of powders used in the present study are listed in Table I.

TABLE I - TYPES AND CHARACTERISTICS OF DIAMOND POWDERS

WARREN GE 300S Metal Bonded Synthetic

- Lot # 711 H-1 (1-2, 2-4, and 4-8 μm)
- Lot # 101 H-4 (2-4 and 4-8 μm)
- Lot # 927 H-9 (10-15 μm)

DAC DeBeers Synthetic

- Lot # S 9225/2 (2-8 μm)
- Lot # S 90237 (10-20 μm)

DAC DeBeers Natural

- Lot # N 9226/1 (2-8 μm)
- Lot # N 91168 (10-20 μm)

Dubble Dee Harris 300 S Synthetic

Mix (I)
- Lot # 1119H-12 (0 - 1/2 μm)
- Lot # 622I-4 (1/2 - 1 μm)
- Lot # 59I-3 (8 - 12 μm)

Mix (II)
- Lot # 622I-4 (1/2 - 1 μm)
- Lot # 430I-10 (1 - 2 μm)
- Lot # 624I-17 (16 - 20 μm)

The morphology of most widely used diamond powders is shown in the SEM micrographs in Figures 5-8. The typical particle size distribution of some of the powders is shown in Figure 9 (a), (b), and (c). The above listed diamond powders received from the different vendors were all claimed to be of high purity. However, in some batches metallic tantalum was detected by EDX analysis. There was no information available on the content of volatiles (particularly moisture) in the diamond powders.

Fig. 5. Morphology of Warren GE synthetic diamond powder. (a) 1000X and (b) 5000X Lot # 101H-4.

Fig. 6. Morphology of Warren GE synthetic diamond powder. (a) 1000X and (b) 2500X Lot # 927H-9.

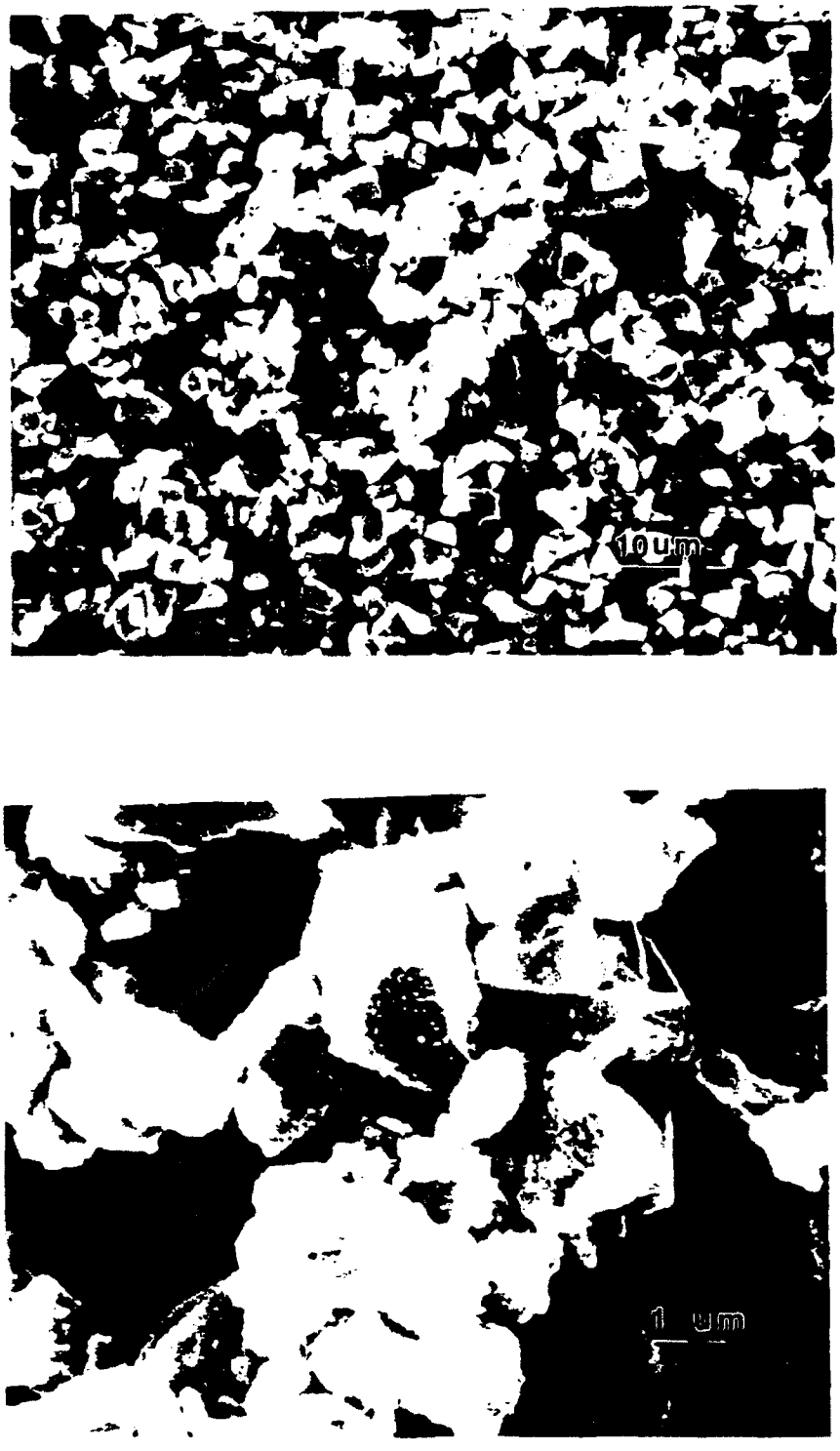

Fig. 7. Morphology of DAC DeBeers synthetic diamond powder (a) 1000X and (b) 5000X (Lot # 9225/2).

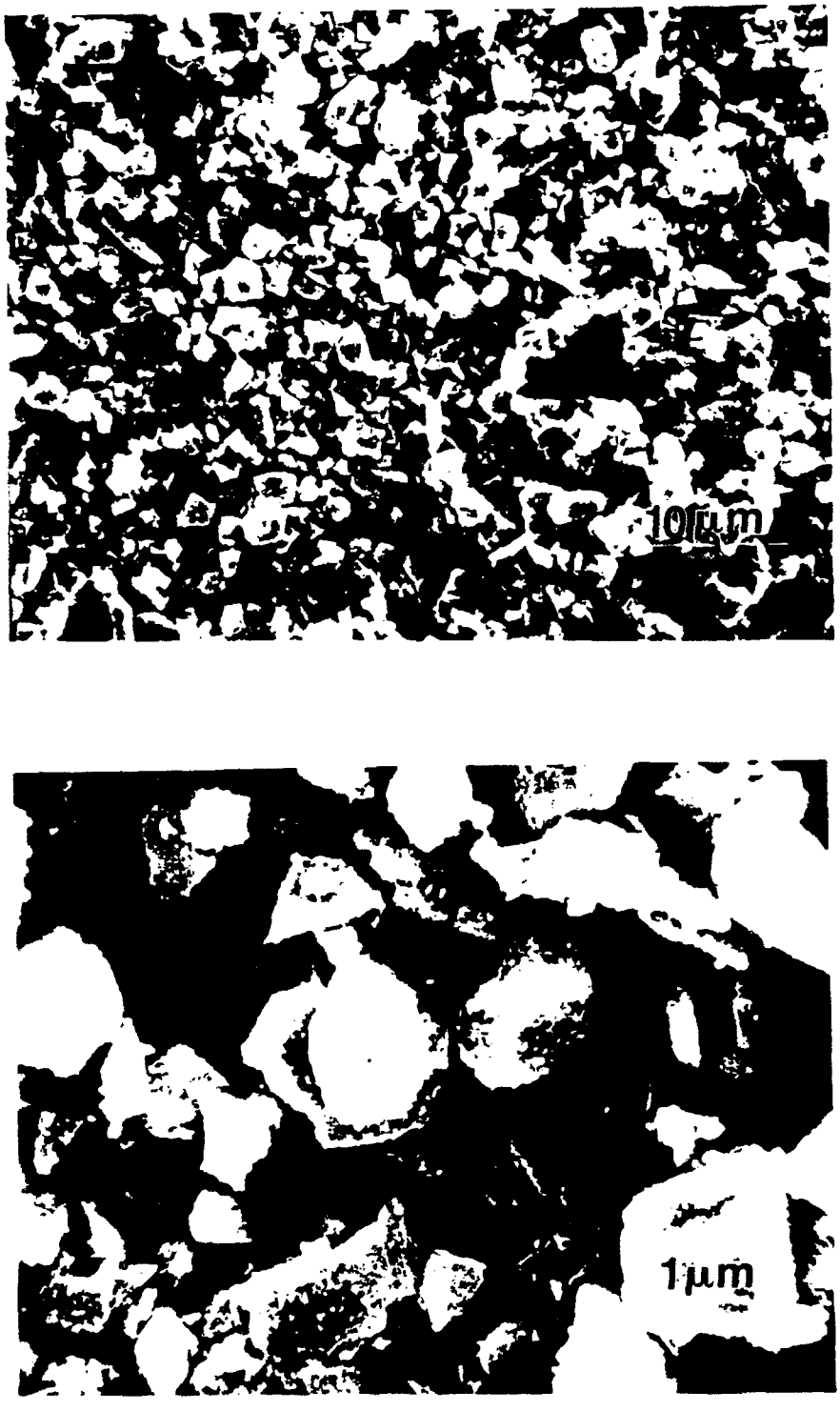

Fig. 8. Morphology of DAC DeBeers natural diamond powder (a) 1000X and (b) 5000X (Lot # 9226/1).

Fig. 9. Morphology of Dubbledee Harris synthetic diamond powder (a) 1000X and (b) 5000X Fine Mix (I).

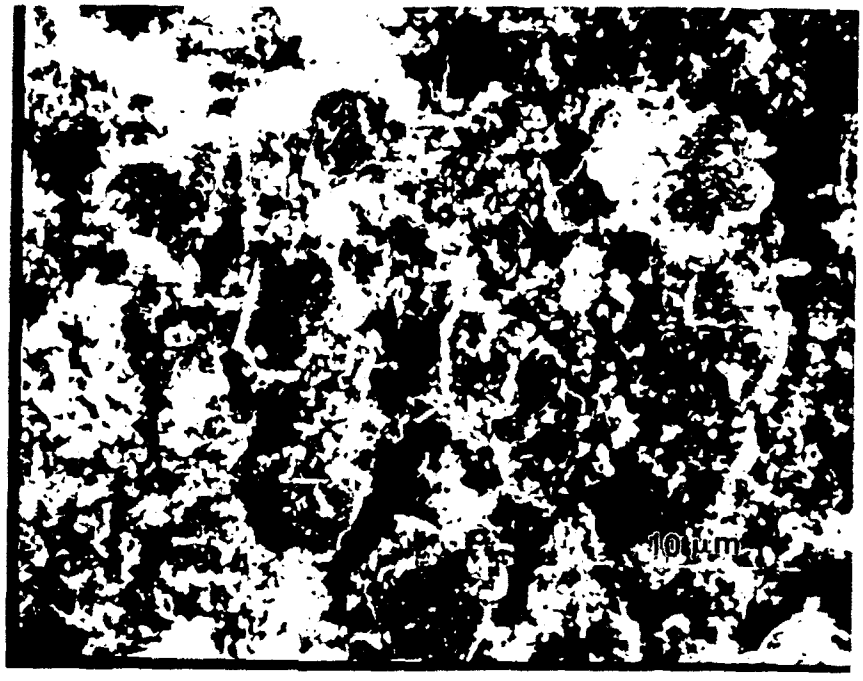

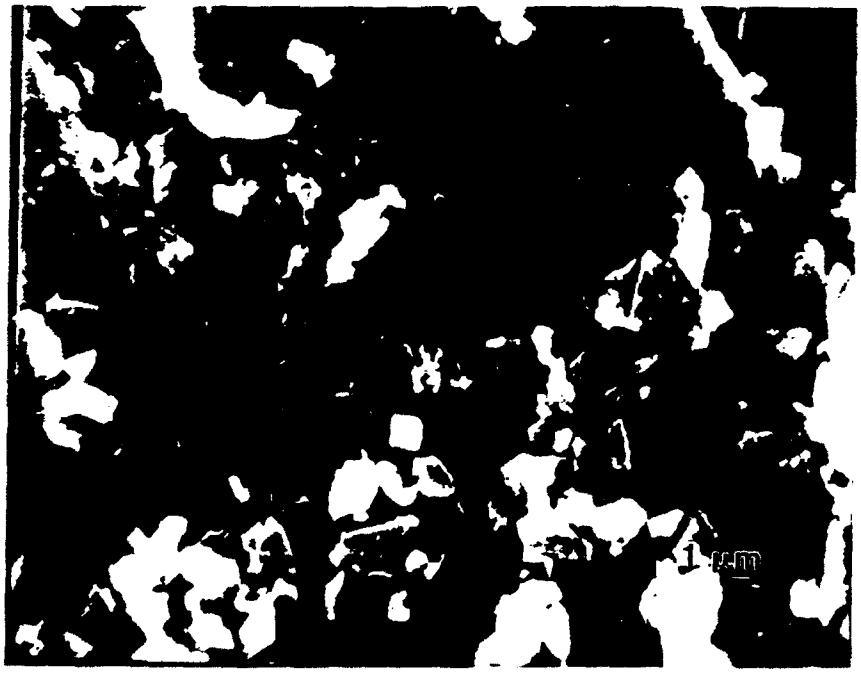

Fig. 9(c,d). Morphology of Dubbledee Harris synthetic diamond powder (c) 1000X and (d) 5000X Coarse Mix (II).

Another aspect explored in this program was pre-compaction treatment of the commercially available diamond powders to assist in the consolidation process. Previous studies have shown that localized surface heating is necessary to produce local melting and particle fusion. To achieve the required surface temperatures, it is also necessary to avoid rapid thermal equilibration of the surface with the particle interior.

It may be possible to substantially improve the fusability of the powders by tailoring the surface morphology to maximize interparticle deformation/friction and heat localization, and thus, assist in bonding. This can be accomplished by either cleansing the surface by heat treatment in vacuum or controlled atmosphere, or by altering the diamond powder surface by oxidation, CVD coating, and flourination. Different types of powder treatments used in the present study are listed in Table II.

TABLE II - DIAMOND POWDER TREATMENTS AND COATINGS

(a) Annealing at 800°C for 8 hours in flowing Ar gas

(b) Baking at 200°C for 5 hours in 100 μm vacuum

(c) Surface oxidation of diamond particles at 800°C for 1 hour

(d) Mixing of diamond powders with additives such as C_{60} and Cu

(e) Coating of powders with C_{60} dispersed in toluene

(f) Fluorination of diamond powders

Flourination of the diamond powders was performed with the assistance of Mr. John D. Hewes collaborating with Dr. Zafar Iqbal at Allied-Signal, Inc. The objective of the flourination treatment was to replace the oxygen ions with flourine ions on the surface. To the best of our knowledge this is the first flourination study of diamond powders ever attempted.

The diamond powders were flourinated in a monel tube fitted with 316 SS elbows/reducers, thoroughly cleaned using detergent/water/methylene chloride/methanol. The cleansed tube is placed in a Lindburg 13305 tube furnace equipped with a Furnatron I temperature controller. After flushing with pre-purified nitrogen at 400°C and cooling to ambient temperature, the monel reactor is loaded with a monel boat and is passivated with flourine gas (Air Products and Chemical Inc., 98+%, purified with sodium biflouride) according to the following schedule:

	DAY 1	DAY 2	DAY 3
1 hr, 3% F_2	50°C	150°C	300°C
1 hr, 5% F_2	50°C	150°C	300°C
1 hr, 20% F_2	50°C	150°C	300°C
1 hr, 45% F_2	50°C	150°C	300°C
18 hr, 100% F_2	50°C	150°C	300°C

The monel boat is then removed from the reactor and placed inside a freshly regenerated Ar-filled glove box containing 0.89 g of the diamond powder. The boat is filled with the powder and again placed in the reactor tube under a strong flow of nitrogen gas. The diamond powder is dried for about 15 minutes at 700°C under a flow of nitrogen (ca. 15 sccm). Upon cooling to 250°C, F_2 diluted with N_2 is admitted into the reactor according to the following schedule:

1 hr	1% F_2	@	200 sccm
1 hr	3% F_2	@	200 sccm
0.5 hr	6% F_2	@	200 sccm
0.5 hr	12% F_2	@	200 sccm
0.5 hr	25% F_2	@	100 sccm
0.5 hr	50% F_2	@	50 sccm

The reactor is cooled to ambient temperature under nitrogen flow. The sample is removed inside a nitrogen-filled glove bag and transferred to a glove box. XPS analysis indicated that the diamond powders contained 83.5 atom% C, 15 atom-% F, and 1.5 atom-% O. A comparison of XPS traces of untreated, flourinated, and flourinated+air exposed diamond powders is shown in Fig. 10.

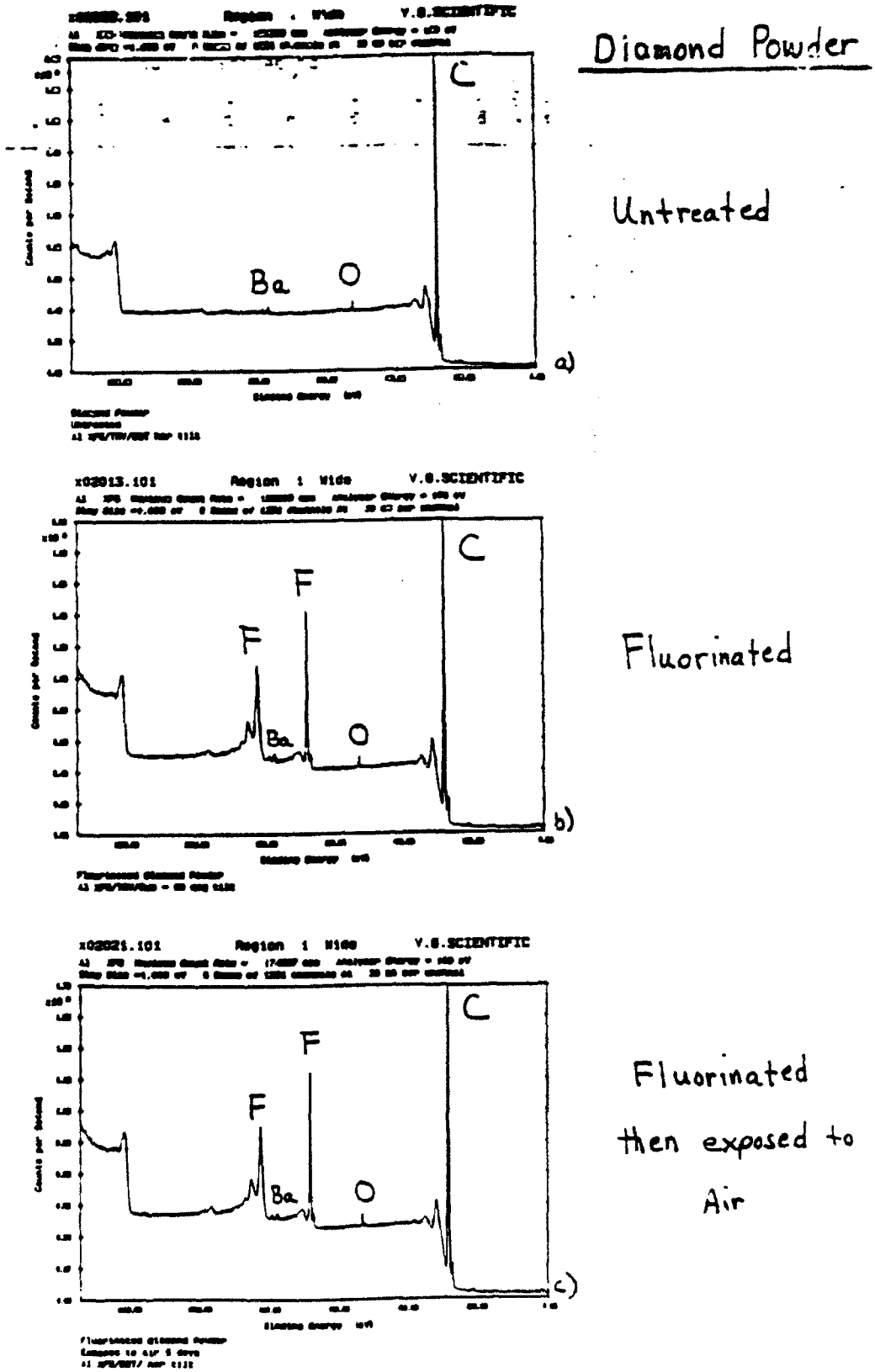

Fig. 10. XPS traces of (a) untreated, (b) flourinated, and (c) flourinated + air exposed diamond powders.

2.2 Shock Compaction Experimental Assemblies

A variety of techniques[18] employing explosive detonation or gun impact techniques can be used to produce shock waves of the desired amplitude and duration for diamond powder consolidation. In the present work, the well-calibrated CETR/Sawaoka plate impact system, shown schematically in Figure 11, was used. The system consists of twelve powder containing 304 stainless steel capsules, embedded in a stainless steel target plate backed by another momentum trapping steel plate. A plane-wave lens is used to detonate the main explosive (PBX 9404) pad of desired thickness and accelerate a flyer plate to impact the capsule assembly. The plane wave lens contains two types of explosives: an outside detasheet explosive of a faster detonation velocity (D_f) and an inside emulsion explosive of slower detonation velocity (D_s). Upon maintaining the cone angle equal to $\sin^{-1}\ (D_f/D_s)$, a planar detonation front is initiated in the main explosive.

The flyer-plate impact velocity can be calculated using the simplified Gurney-Kennedy equation,[23,24] which considers the chemical energy of the explosive to be transformed into the kinetic energy of the explosive products and the metal fragments. The analysis yields the terminal velocity of the flyer plate, v_o, as a function of the ratio of the mass of metal flyer plate (M) and explosive charge mass (C). Therefore,

$$v_o = \sqrt{2E}\sqrt{\frac{3}{1 + 5\left(\frac{M}{C}\right) + 4\left(\frac{M}{C}\right)^2}} \qquad (5)$$

where, $\sqrt{2E}$ is the Gurney energy (in units of velocity). The impact velocity and planarity can also be measured using a network of contact pins placed across the impact surface at different heights. The flyer arrival time at different pins heights and positions gives the impact velocity and planarity.

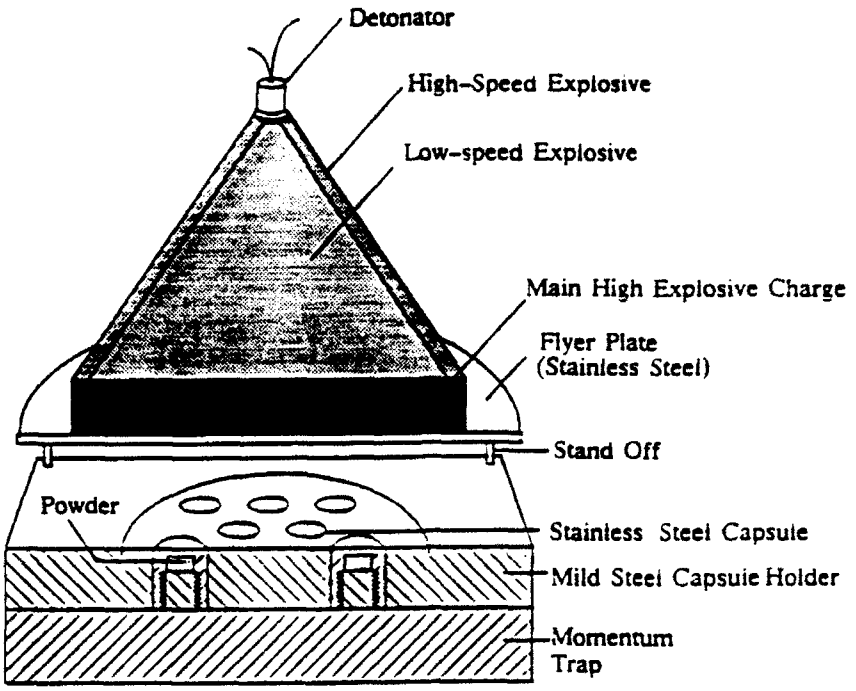

Fig. 11. Schematic of the CETR/Sawaoka 12-capsule shock recovery fixture configuration and explosive loading system.

Cylindrical compacts (12 mm diameter by 1-5 mm thick) are produced with this system. The system is particularly suitable for conducting high-pressure recovery experiments (at 10-100 GPa), and has the advantage that it can create, at one time, 12 different combinations subjected to similar shock conditions. However, with such an assembly, 2-D effects can dominate the loading process within the low-density powders encapsulated in solid steel containers, resulting in radial focussing and generation of extreme pressures along the compact axis. Fig. 12 shows 2-D simulations of variation of shock pressure and mean-bulk temperature with time for 55% dense rutile at 1.9 km/s.[25] Realistic shock conditions actually rely on impact planarity, and the parallelism and flatness of all surfaces normal to the shock.

For diamond powders, 2-D effects may not be so significant due to its high shock velocity, particularly with powders packed at green densities greater than 70% TMD, and also since the compact diameter is significantly larger than the thickness. In such a case a 1-D average pressures can be calculated. Figure 13 shows a typical pressure-time profile for a 2 mm thick 70% dense diamond powder compact, obtained using MY1DL program,[24] the Hugoniot of diamond shown in Fig. 14.

PRESSURE (GPA) CONTOURS FOR 1.9 KM/S

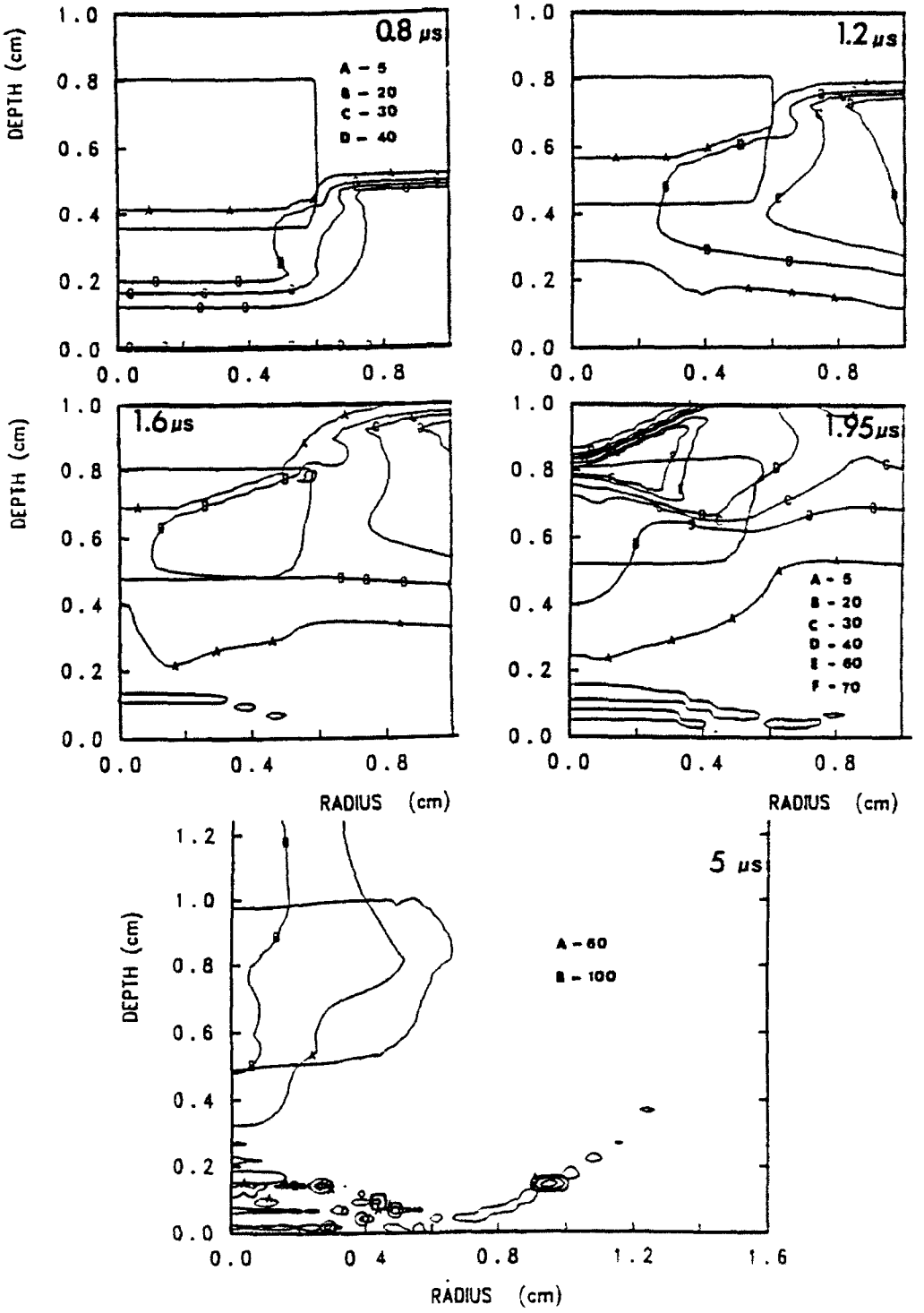

Fig. 12(a). Numerically computed peak pressure contours at different times for 1.9 km/s impact velocity within and in the vicinity of capsule cavity for shock moving from bottom to top.[25]

TEMPERATURE CONTOURS FOR 1.9 KM/S

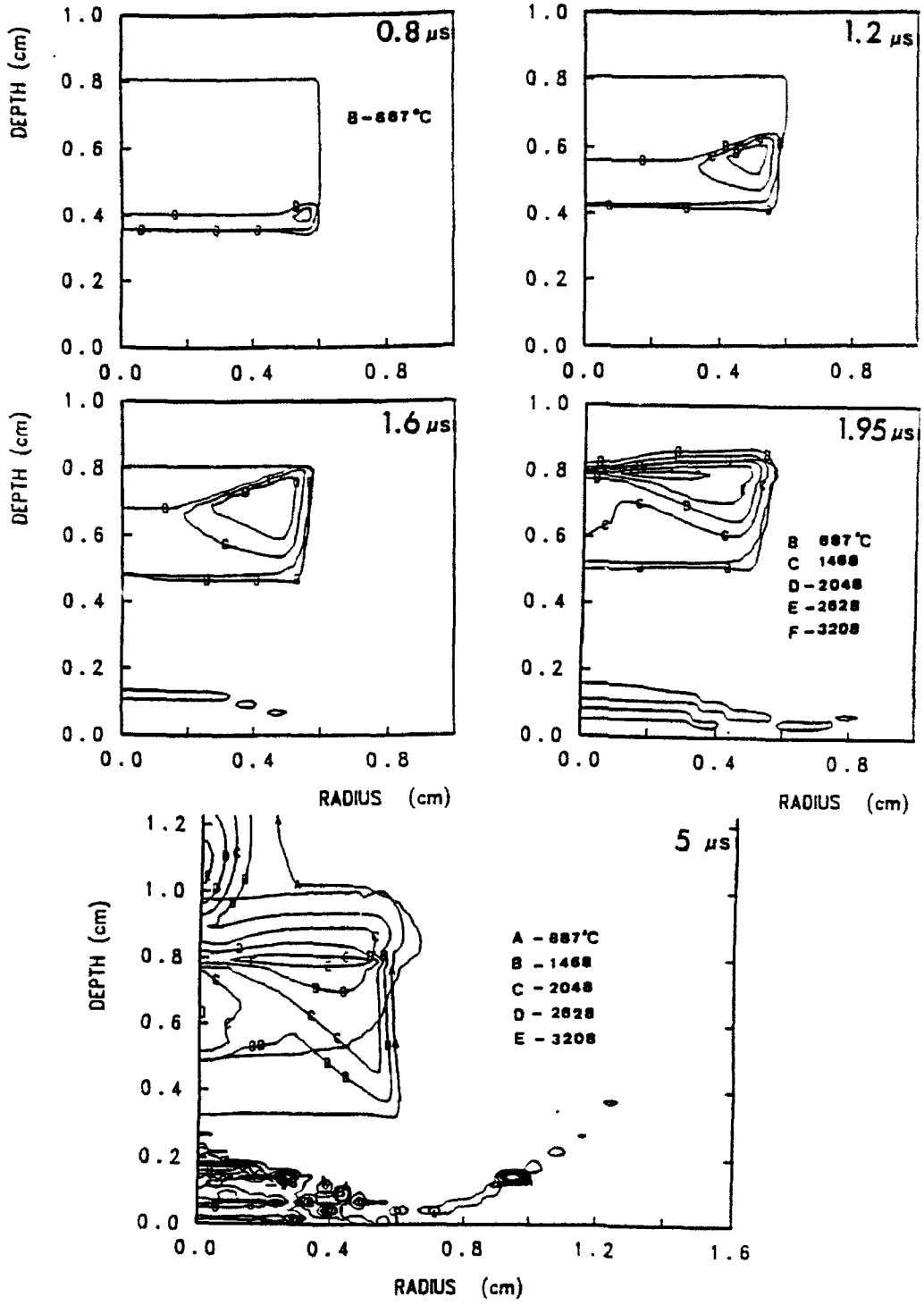

Fig. 12(b). Numerically computed mean-bulk-temperature contours plotted as function of time for 1.9 km/s impact velocity within and in vicinity of capsule cavity for shock moving from bottom to top.[25]

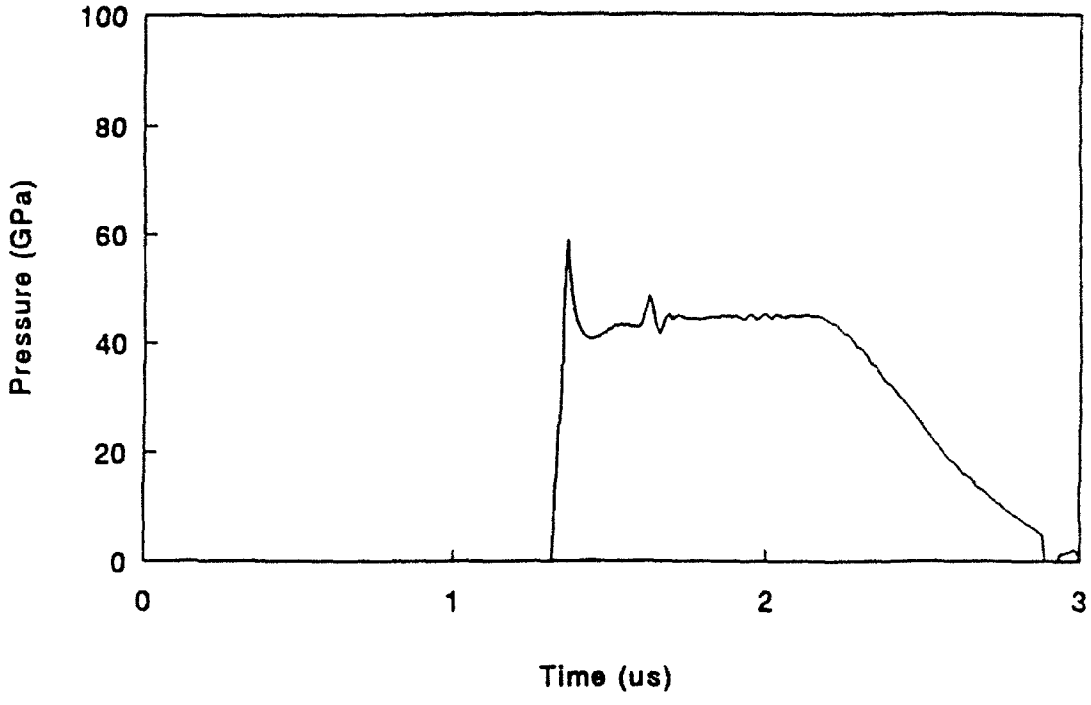

Fig. 13. Typical pressure-time profile for 2 mm thick 70% dense diamond powder compact made at 1.9 km/s velocity.

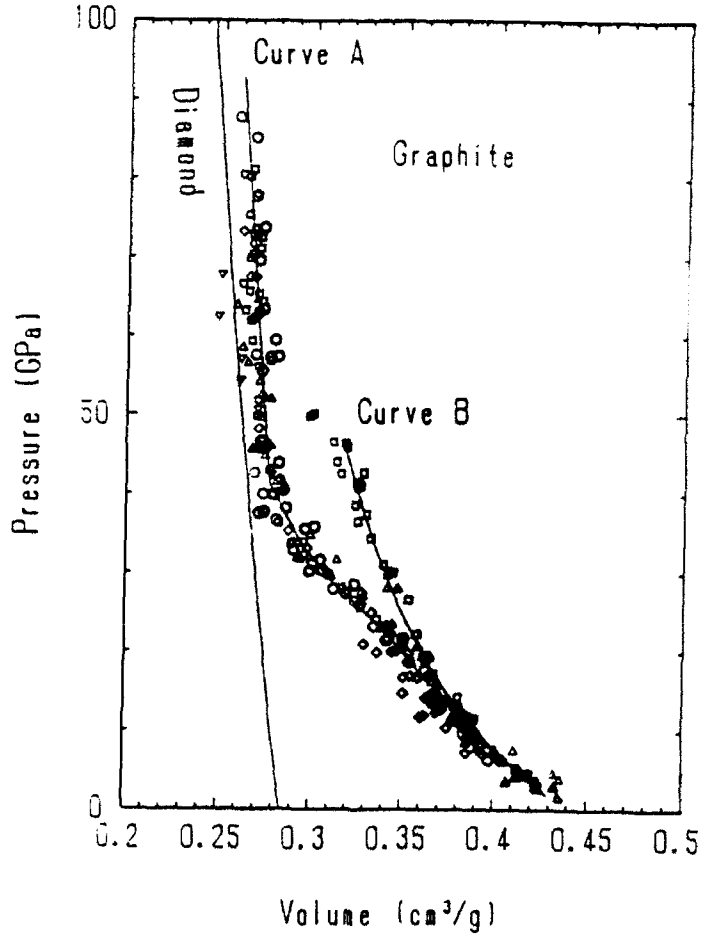

Fig. 14. Pressure-volume Hugoniot of diamond and graphite.

A modification of the twelve capsule system was also adopted in the present work. In this case a four capsule assembly was built to yield 25 mm diameter by 2 mm thick compacts. The impact conditions used were such that shock consolidation conditions similar to the 12-capsule system could be maintained. Figure 15 shows a schematic of the 4-capsule fixture assembly.

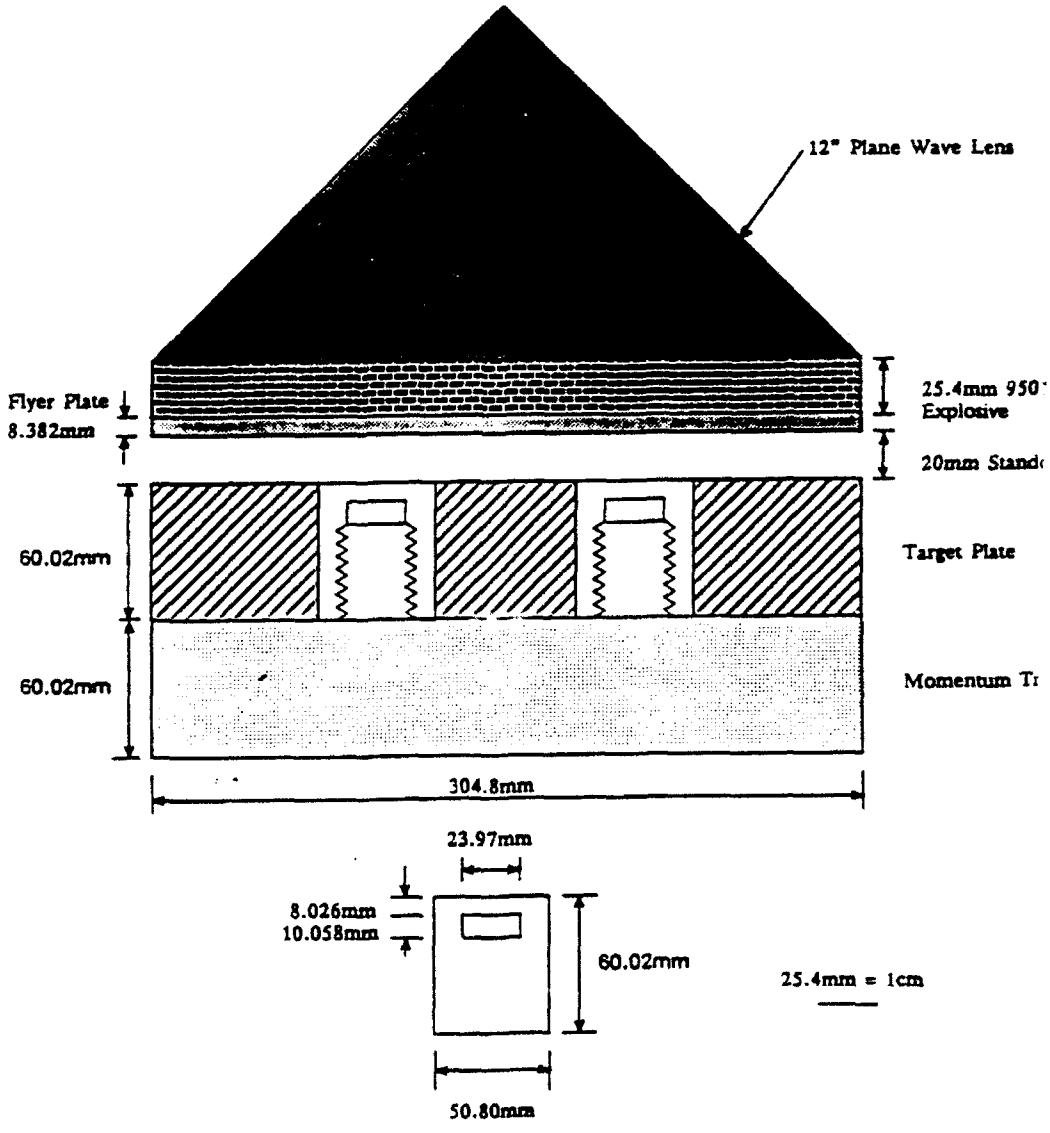

Fig. 15. Schematic of the CETR/Sawaoka 4-capsule shock recovery fixture configuration and explosive loading system.

The shock compaction experiments at CalTech were performed using the 20 mm and 40 mm propellant driven gun systems. The target fixture was especially designed to allow safe recovery of the shock compacted samples made at impact velocities greater than 1.5 km/s. A schematic of the target container fixture is shown in Figure 16. The advantage of this system is that it enables the consolidation experiments to be performed under controlled vacuum or inert atmosphere.

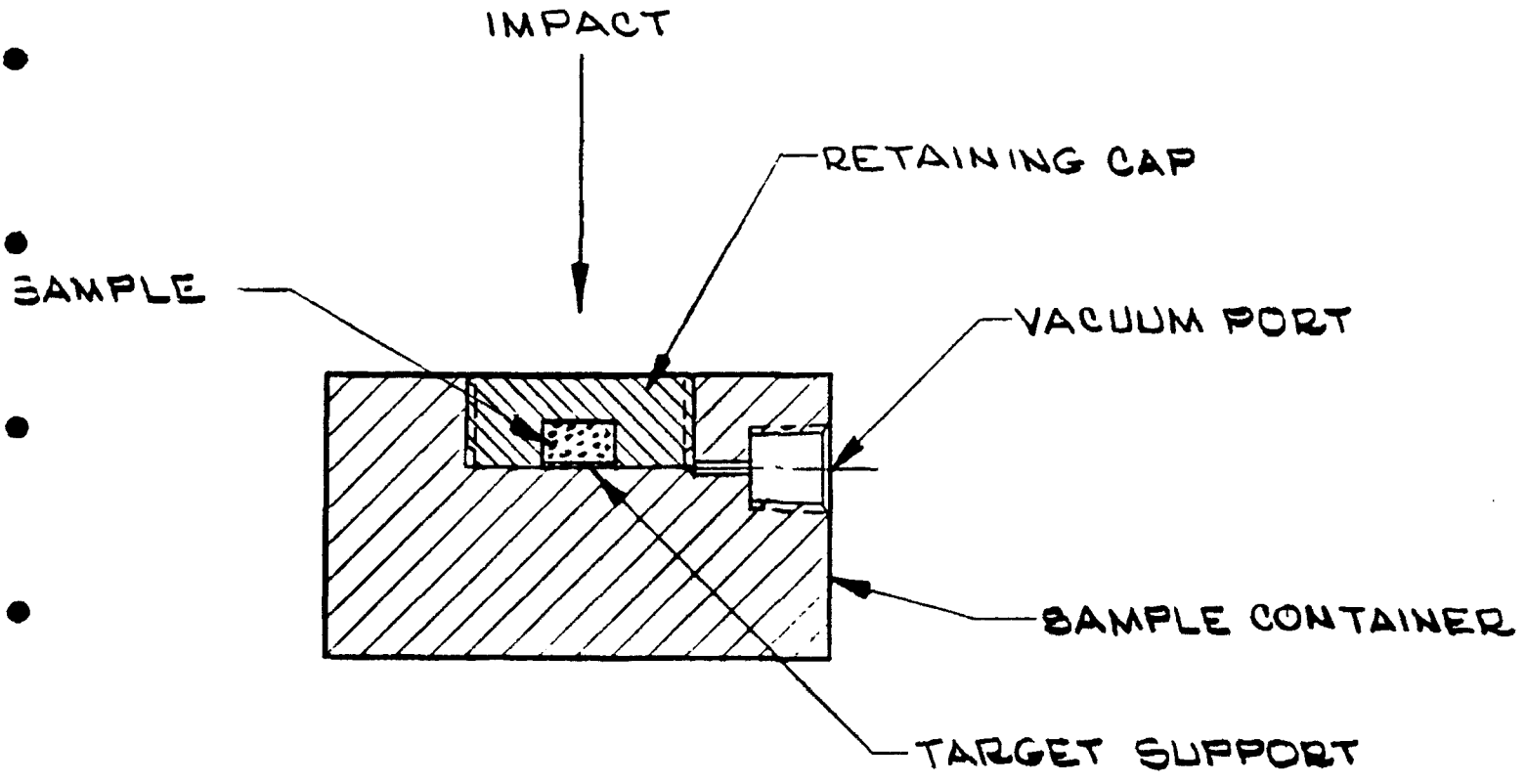

Fig. 16. Schematic of the CalTech target recovery fixture used with the 20 mm and 40 mm propellant driven gun systems.

2.3 Diamond Compact Recovery and Characterization

The shock consolidated diamond compacts were recovered by carefully machining the steel capsules. The compacts were then ground using diamond micro-grid to obtain parallel surfaces. Density measurements were made using Archimedes method. The compacts were initially characterized under a low magnification stereo microscope for general appearance. The surface roughness of the compacts was monitored by SEM analysis. SEM coupled with EDX analysis was also performed to provide information regarding phase purity of both the diamond powders as well as the bulk and surface regions of the diamond compacts.

Raman scattering spectroscopy was used together with x-ray diffraction to determine phase purity of diamond compacts. The presence of diamond phase is signalled by appearance of a sharp resonance at 1332 cm^{-1}. Raman scattering is also sensitive to the presence of graphite and other disordered carbon forms. Using cross-sectional corrections and peak widths the volume fraction of diamond and residual strain in the compacts can be determined.

Electrical resistivity measurements were performed using the four-probe technique, with both AC and DC currents. A variable temperature substrate holder was employed to measure the electrical resistances at various positions on the compacts.

Thermal conductivity of the diamond compacts was determined by an indirect method employing phonon velocity and correlating it to the thermal conductivity of diamond using the Debye formula for dielectric solids. A direct measurement of conductivity was also made using the laser pulsed photothermal radiometry technique generally applicable for thin samples.

CHAP. 3 - RESULTS OF SHOCK COMPACTION EXPERIMENTS

Shock compaction experiments were performed using explosively accelerated plate-impact assembly at New Mexico Tech and propellant driven 40 mm gun system at CalTech. Experiments on diamond powders of different types, particle morphology, size distribution, and surface treatment, were done at an impact velocity range of 1.5-2.1 km/s. The initial porosity of the green compact and peak pressure determine the total shock energy input into powders. Thus, the greater the initial porosity the larger are the bulk and surface temperatures. Rapid cooling from the shock temperature can generate thermal stresses and possibly induce cracking of the diamond compacts, and long thermal excursions can make diamond-to-graphite transition possible.

The goal in shock compaction of diamond powders, is thus, to input just sufficient shock energy to fuse the powders without causing long thermal excursions, and thereby prevent formation of non-diamond (graphite or amorphous carbon) phases. High initial packing densities (65%-75% TMD), obtained via use of powders with appropriate particle size distribution can minimize long-term temperature exposures. Introducing texture or non-thermally conducting coating on diamond particles can allow energy localization and heat retention. Thus, with the use of optimal powder packing and surface treatments, it may be possible to remain in the narrow window of energy required for interparticle fusion without conversion of interface layer to non-diamond phases.

3.1 Powder Rheology and Compressibility

Physical and rheological characterization work on diamond powders was done at CalTech. Typical apparent and tap densities, and friction index, of diamond powders before and after surface are listed in Table III. An example of static powder loading curves for DAC DeBeers synthetic powder in as-received and oxidation state, shown in Fig. 17, reveals the modified static com-

pressibility, due to altered surface characteristics, which can affect the flow and packing characteristics of the powders.

TABLE III - MEASURED RHEOLOGICAL PROPERTIES OF DIAMOND POWDERS

POWDER	TAP DENSITY (g/cc)	APPARENT DENSITY (g/cc)	FRICTION INDEX
GE SYN, 1-8 μm	1.36	0.85 the	1.60
DAC DeBeers NAT, 1-10 μm	1.68	1.11	1.51
DAC DeBeers SYN, 1-10 μm	1.63	1.05	1.55
GE SYN, 1-10 μm	1.74	1.19	1.46
GE SYN, 1-8 μm	1.62	0.98	1.65
GE SYN, 0.5-2 μm	1.27	0.76	1.67
Oxidized GE SYN, 1-8 μm	1.06	0.56	1.90
Oxidized DeBeers NAT 1-10 μm	-	0.24	-

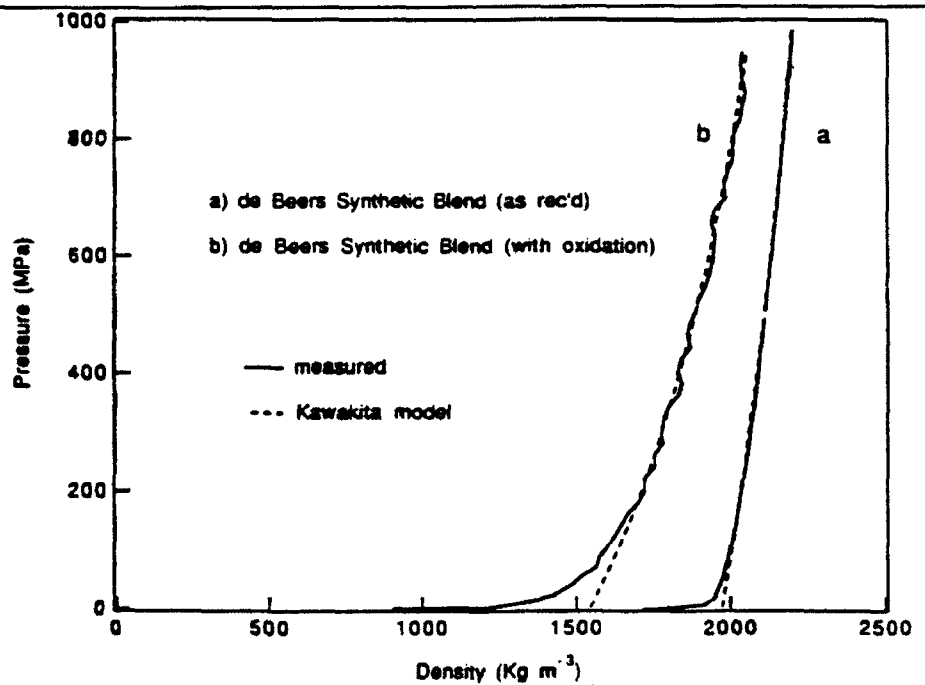

Fig. 17. Pressure-density compressibility curves of as-received and surface oxidized DeBeers synthetic powder.

3.2 Experimental Results

A brief summary of the various shock compaction experiments conducted using the explosive system, along with experimental conditions and the main variables studied is listed in Table V. More specific details are provided in the sample by sample tabulation of all experiments in Appendix - A.

The compacts recovered after machining the samples were ground and polished by standard techniques. Density measurements were performed on the various compacts using the Archimedes method. Comparisons were also made with a CVD made diamond piece which had a density of 3.48 g/cc. The density measurements are reported in the detailed tabulation of the sample/experiment listing in Appendix - A. Densities of the various compacts are also plotted as a function of initial packing density in Figure 18 (a), (b), and (c) for each of the three different powder types: Warren GE synthetic, DAC DeBeers natural, and DAC synthetic diamond powder compacts. It is seen that for each powder type, initial packing densities below 65% consistently result in final densities < 75%, while for packing densities greater than 65%, the final compact densities range between 85% - 94% TMD.

Increasing the impact velocity from 1.7 to 1.9 km/s, and therefore the shock consolidation conditions, results in improved densification with final compact densities increasing from 70-75% to the 88-94% TMD range. However, a further increase in shock conditions does not lead to any more densification. A typical variation of final compact density with impact velocity for the DAC DeBeers natural diamond powder is shown in figure 19.

The diamond compacts were also characterized via electrical resistance measurements. A fixture consisting of two probes set 5 mm distance apart was built. Plots showing the typical variation of ohmic resistance as a function of final compact density for the DAC DeBeers natural and synthetic and the Warren GE synthetic powder compacts are shown in Fig. 16 (a) - (c).

TABLE V - SHOCK-COMPACTION EXPERIMENTAL CONDITIONS

Shot No.	Impact Vel	Powder Type/characteristic	Recovery/Variables
NMG 9114	1.89 km/s	Warren 300 S, DAC Syn & Nat	8 of 12 recovered; as-rec'd blew, Ar-treated and powders sandwiched between reactive mixtures recovered
NMG 9115	1.68 km/s	Warren 300 S, DAC Syn & Nat	12 of 12 recovered including as-rec'd, Ar-treated, and sandwiched between Al_2O_3 and W powder laminates
NMG 9124	1.90 km/s	Warren 300 S, DAC Syn & Nat	11 of 12 recovered including Ar-, oxidation-, vacuum-treated, and C_{60} coated; one C_{60} coated lost
NMG 9125	1.90 km/s	DAC Syn and Nat	4 of 4 Ar- and Vacuum-treated powders recovered in form of 1" dia compacts with extensive cracking
NMG 9131	2.15 km/s	Warren 300 S, DAC Syn and Nat	6 of 12 recovered; higher pressure experiment, powders were Ar- and vacuum-treated, and were of varying particle size distribution
NMG 9132	1.90 km/s	Warren 300 S, DAC Syn and Nat	4 of 4 Ar- treated recovered in form of 1" dia compacts with extensive cracking
NMG 9201	1.90 km/s	Warren 300 S, DAC Syn and Nat	6 of 12 recovered; powders were Ar- and oxidation-treated, and were of varying packing density
NMG 9202	1.90 km/s	Warren 300 S, DAC Syn and Nat	4 of 4 treated; Ar-treated powders of different size distribution to yield high packing density
NMG 9213	1.84 km/s	Warren 300 S, DAC Syn and Nat	11 of 12 recovered, Ar-treated powders of different size distributions to yield high packing density
NMG 9240	1.90 km/s	Dubble Dee Harris 300 S	12 of 12 recovered, Ar-treated powders of various controlled size distributions to yield maximum packing density

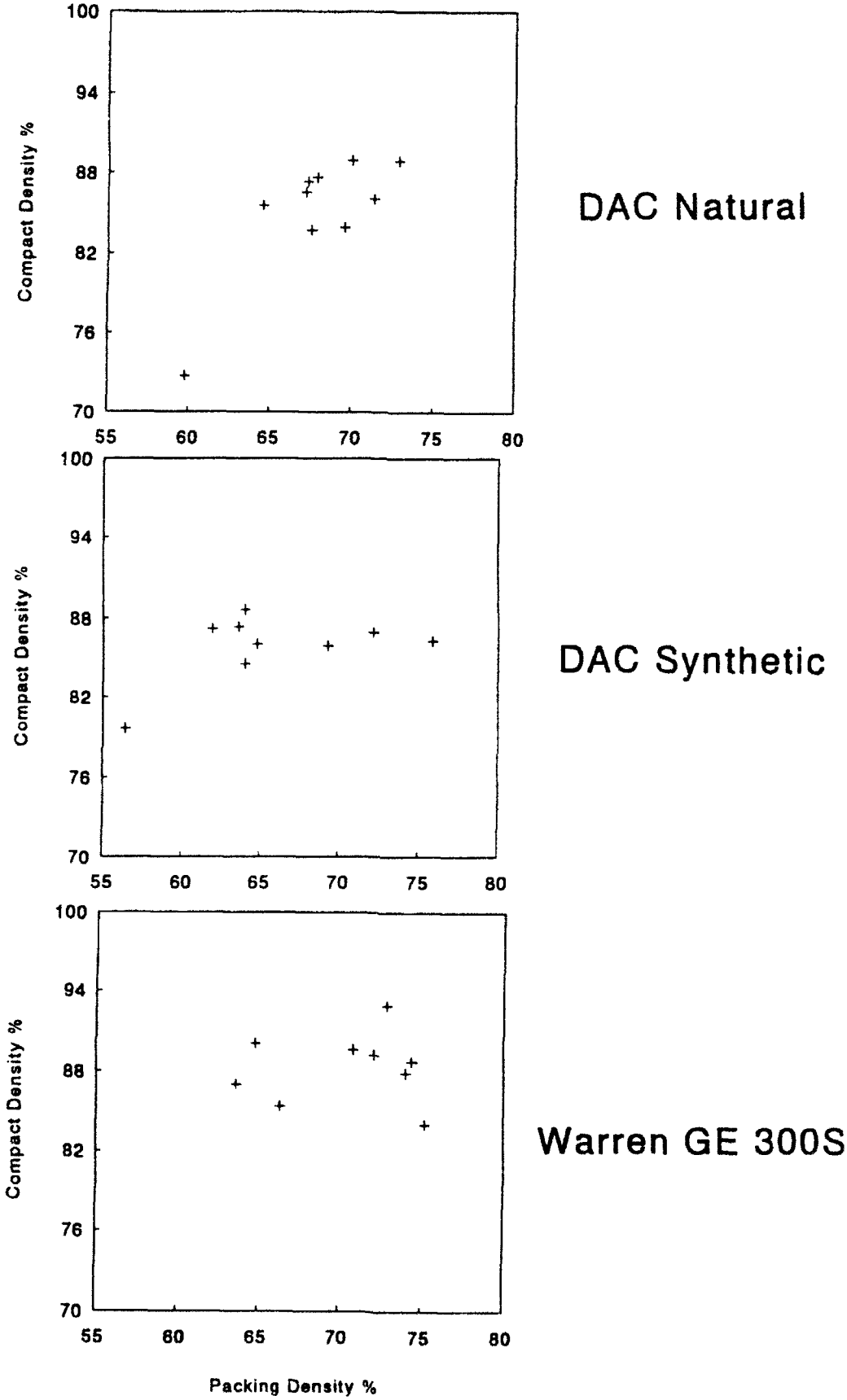

Fig. 18. Plots of variation of final compact density as function of initial packing density for (a) DAC natural; (b) DAC synthetic; and (c) Warren GE synthetic diamond powders.

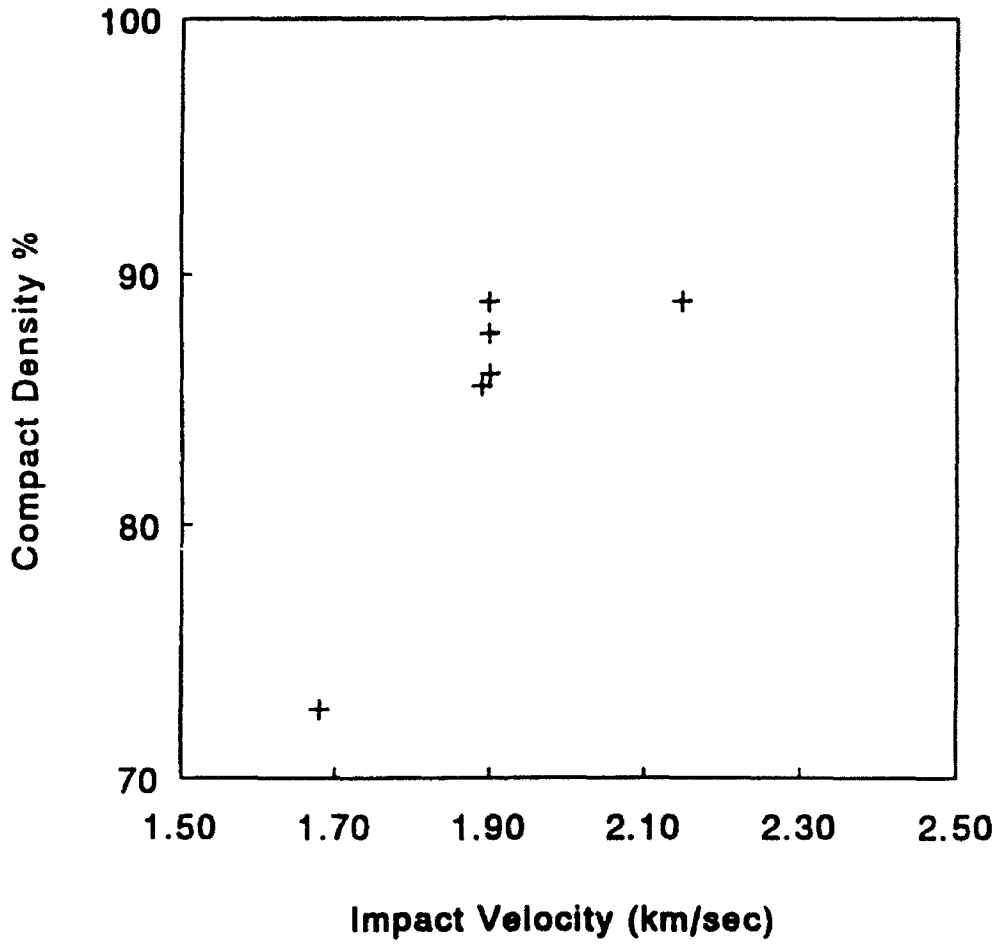

Fig. 19. Plot of variation of final compact density as a function of the impact velocity for the DAC DeBeers natural diamond powder.

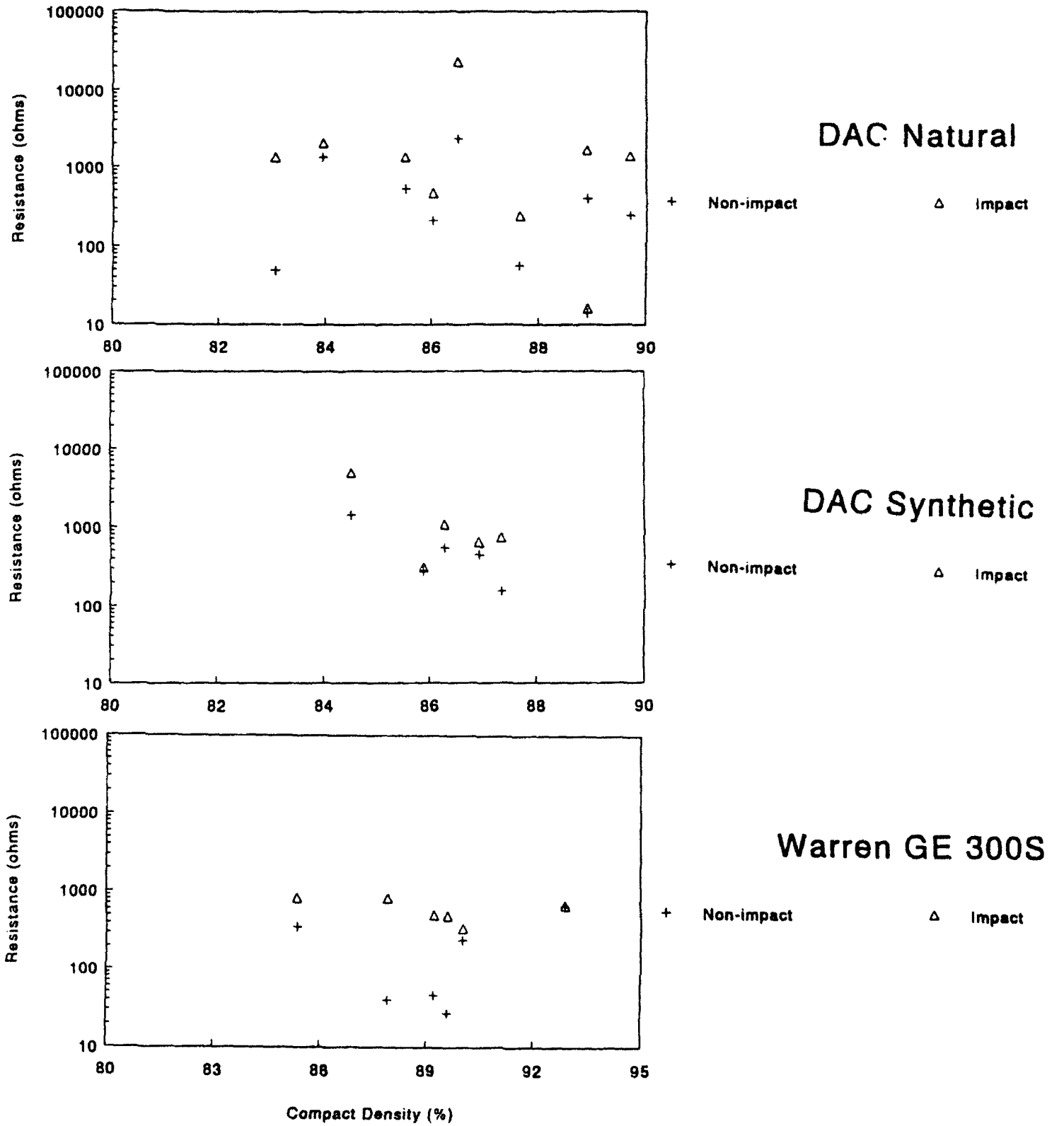

Fig. 20. Plots of variation of ohmic resistance as a function of the final compact density for (a) DAC natural; (b) DAC synthetic; and (c) Warren GE synthetic diamond powders.

CHAP. 4. - MICROSTRUCTURAL CHARACTERISTICS OF DIAMOND COMPACTS

In order to infer the presence of non-diamond (graphitic or amorphous carbon) phases, several types of microstructural characterization techniques were adopted, including SEM analysis, x-ray diffraction, and Raman spectroscopy. The results of these analysis will be presented in the following subsections.

4.1 Scanning Electron Microscopy (SEM) Analysis

The recovered diamond compacts (12 mm diameter by 1-2 mm thickness) were characterized by SEM analysis to identify specific features present on the polished surfaces of the compacts as well as on the cross-section surfaces of fractured compacts. Microphotographs of typical polished impact and non-impact surfaces of the DAC DeBeers synthetic diamond powder compact (sample # 9131-10) are shown in Figure 21 (a) and (b).

An SEM image sequence (at different magnifications) of the typical surface of this compact is shown in Figure 22 (a) - (d). The degree of interparticle bonding is more clearly revealed in the higher magnification image sequence shown in Fig. 23 (a) - (d). The fine hair-line type of openings in certain areas of the compacts are actually microcracks, formed perhaps due to stresses generated from thermal quenching effects.

The interparticle phase was more clearly detected by SEM analysis performed on fractured surfaces of compacts. Figure 24 (a)-(d) shows typical fractured surfaces of DAC synthetic diamond powder compact # 9131-10 from two different areas. The rounded voids in (a) and (b) clearly indicate evidence of melt formation and subsequent solidification. The agglomerated fine particulate-like debris around the melted regions appears to contain amorphous material. The micrographs in Fig. 24 (c) and (d) show cleaner interparticle areas and at the same time evidence of deformation structure within particles interiors. Several large melt-like areas were also observed in some of the other compacts.

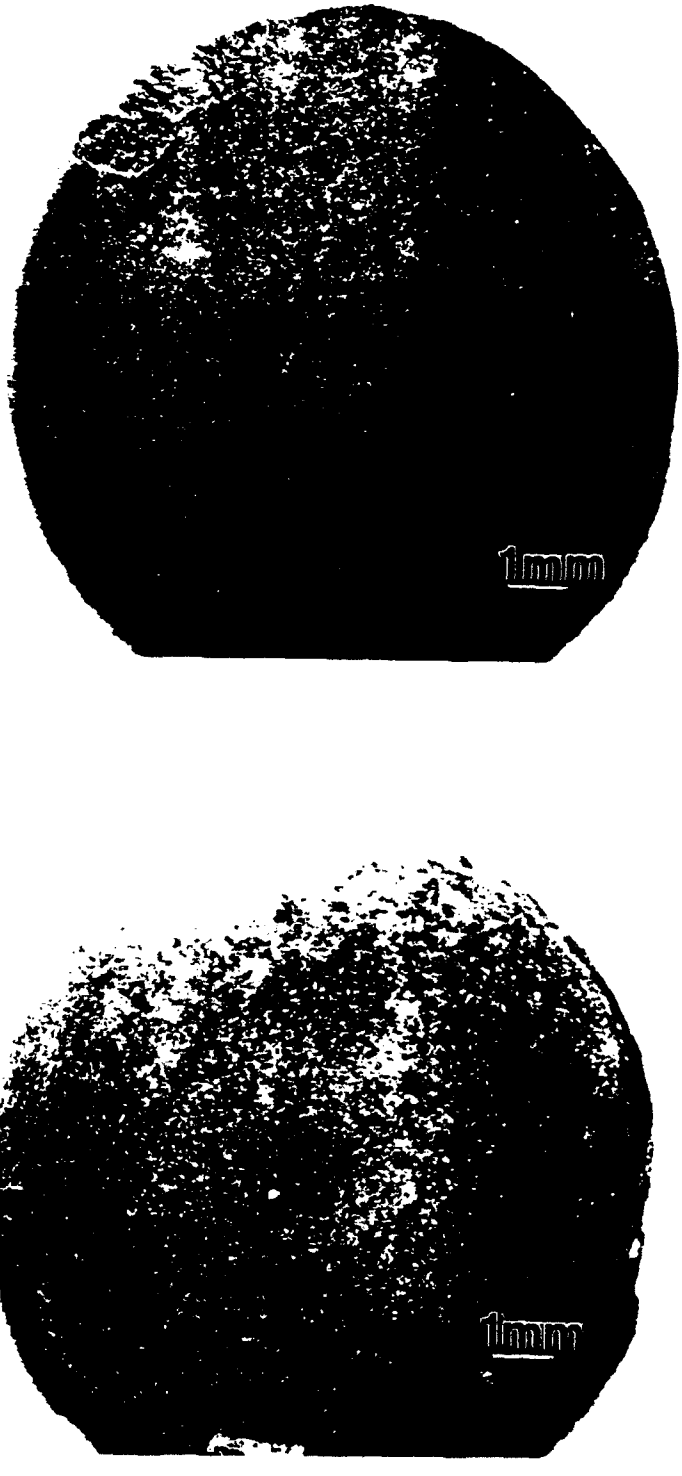

Fig. 21. Microphotographs of polished (a) impact and (b) non-impact surfaces of DAC synthetic diamond compact.

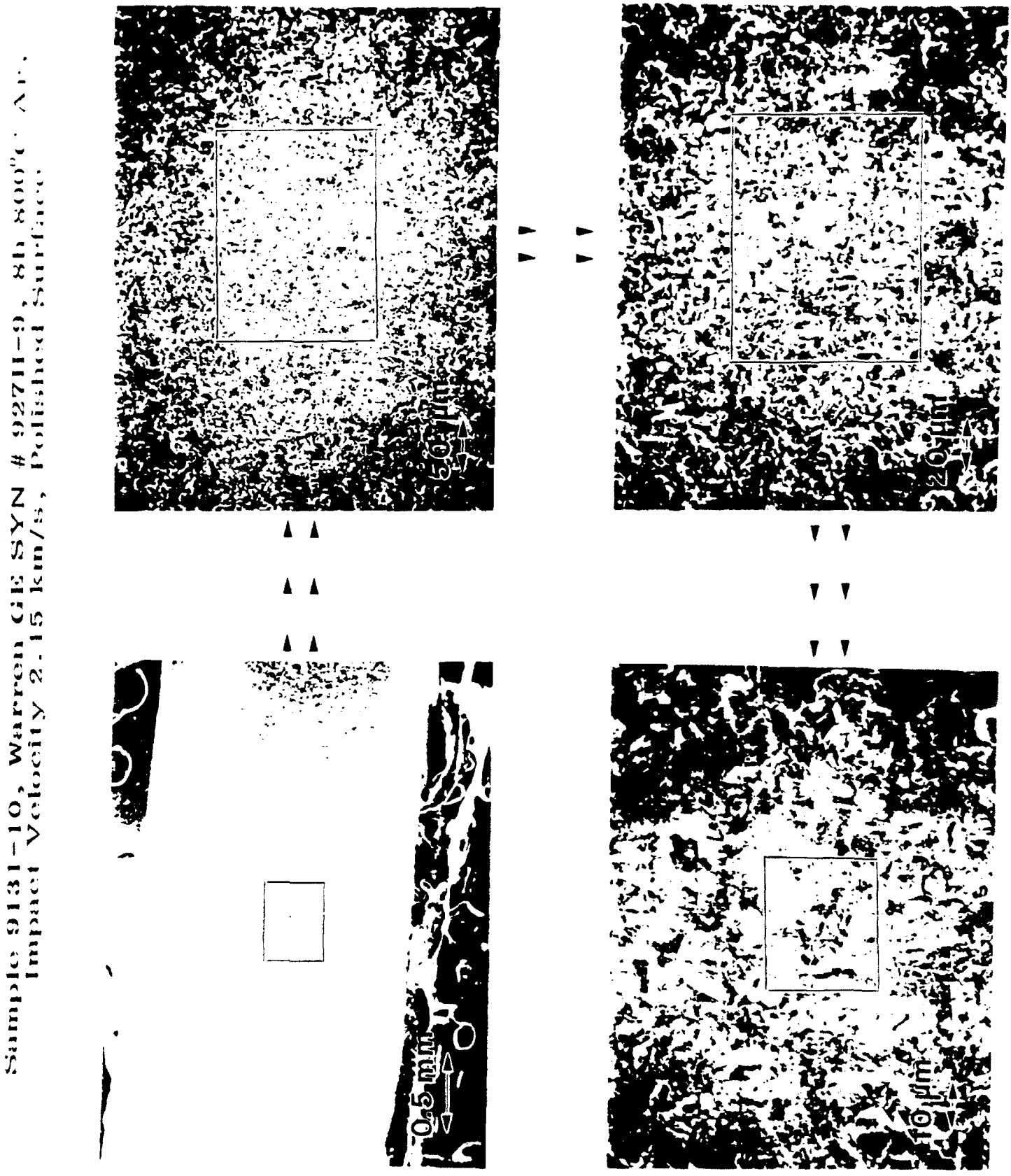

Fig. 22. (a) - (d) SEM image sequence of typical polished surface of compact # 9131-10, at different magnifications.

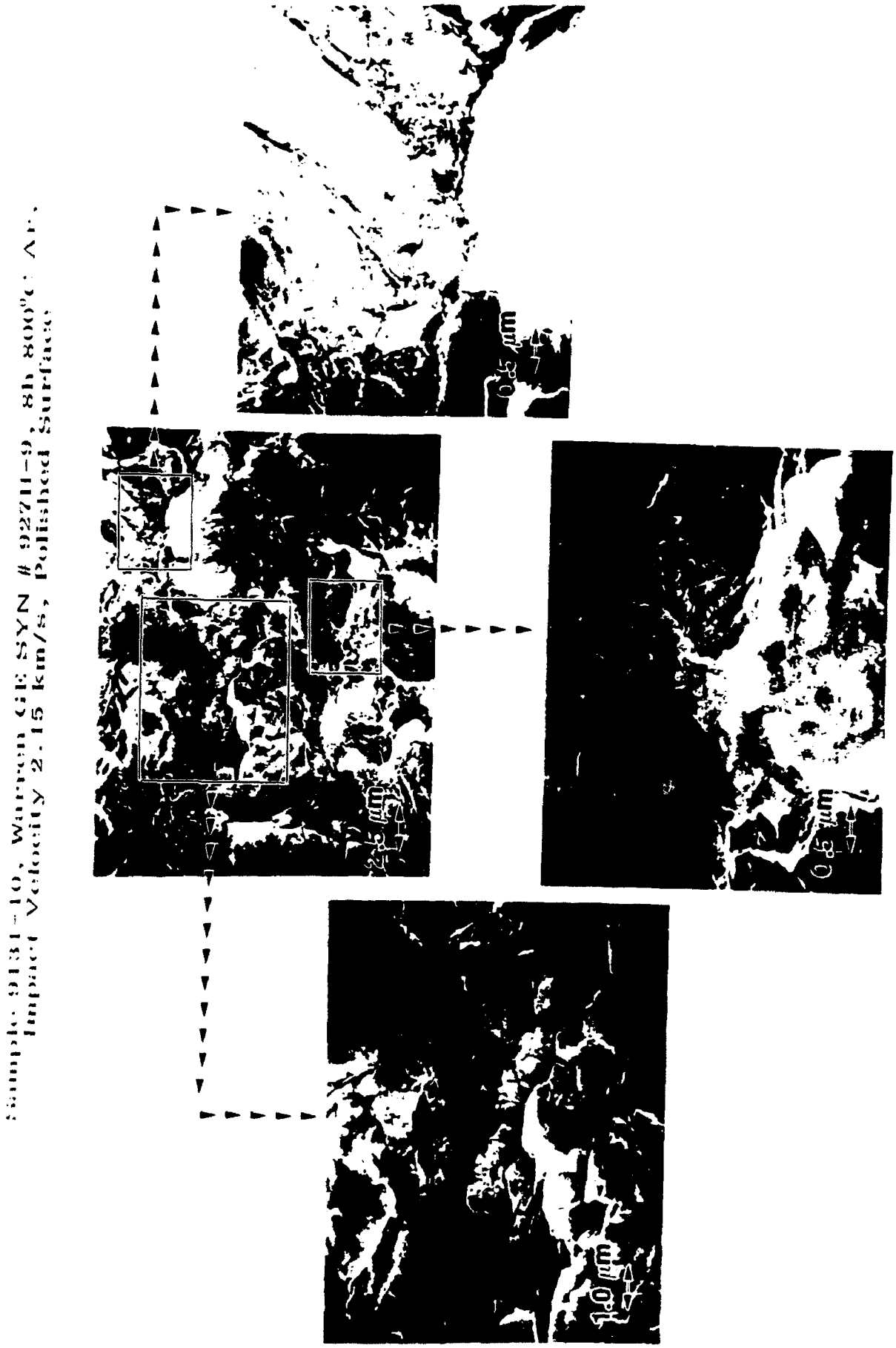

Fig. 23. (a)-(d) Higher magnification SEM image sequence of typical polished surface of compact # 9131-10.

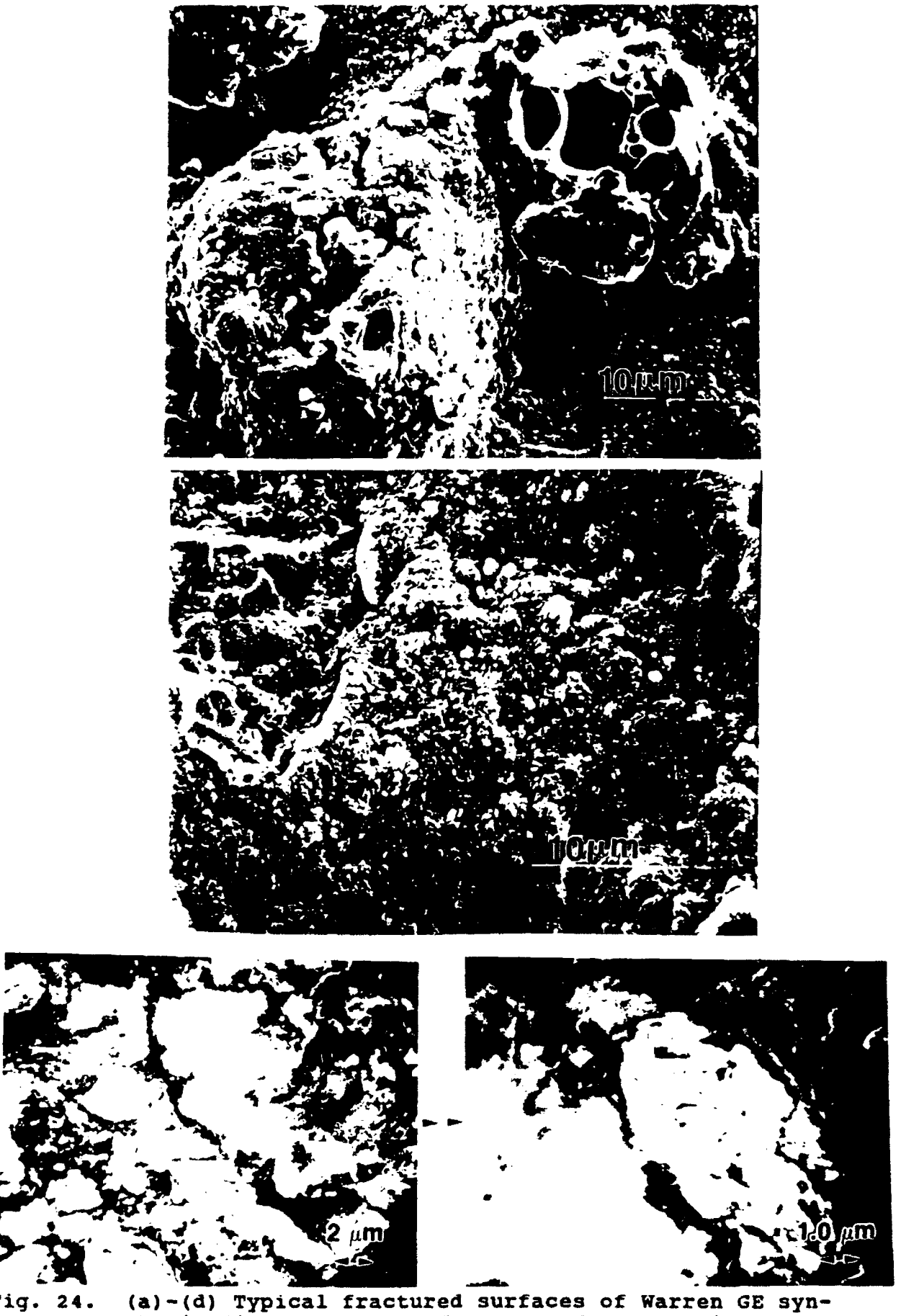

Fig. 24. (a)-(d) Typical fractured surfaces of Warren GE synthetic diamond compact # 9131-10 from two different areas, showing evidence of interparticle melting.

Figure 25 (a) - (e) shows the sequence of low and high magnification SEM images. The melt-like areas are clearly detected at interparticle regions in micrographs (c) and (e). These melt-like areas appear as amorphous regions containing the melted and resolidified material. Some bright contrast crystals are also observed in these melt-like areas, implying perhaps the nucleation and growth of crystalline diamond. The micrographs (b) and (d) show the typical grain structure of the fractured surface. The structure of the grain interior is also seen in Figure 26 (a) - (d) for the Warren GE powder compact # 9213-06. The extensive deformation structure, fine hair-line type microcracks, and in some cases phase separation is evident in these micrographs.

Energy dispersive x-ray analysis performed in these melt-like areas also revealed the presence of metallic tantalum, along with some other alkaline impurities. The presence of impurities can allow retention of heat at interparticle regions for prolonged times, thereby permitting formation of the liquid phase and its subsequent slow transformation to amorphous or graphitic carbon instead of cubic diamond.

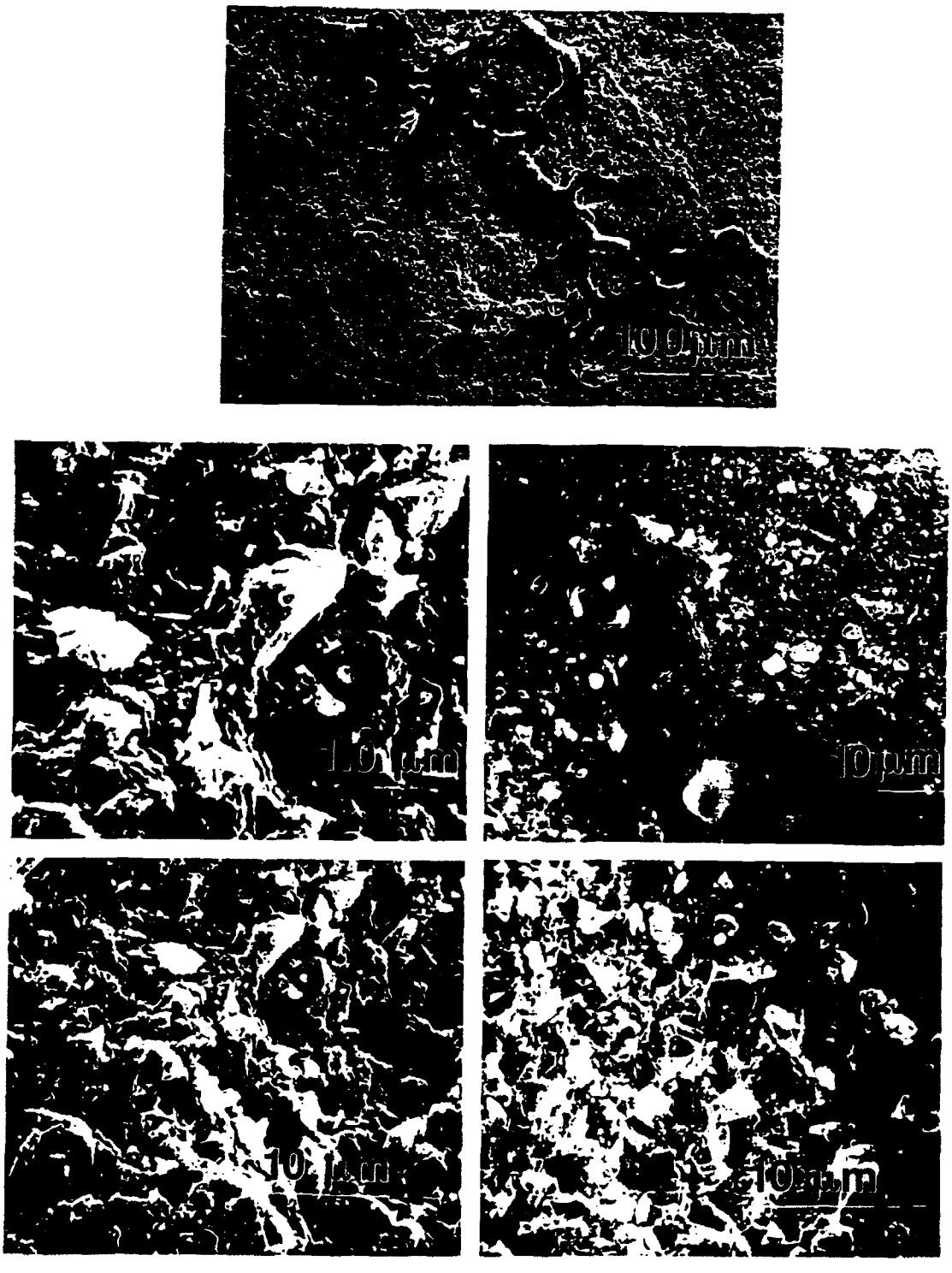

Fig. 25. (a)-(e) Low and high magnification SEM image sequence of typical fracture surfaces of DAC synthetic diamond compact # 9124-10, showing interparticle melt areas.

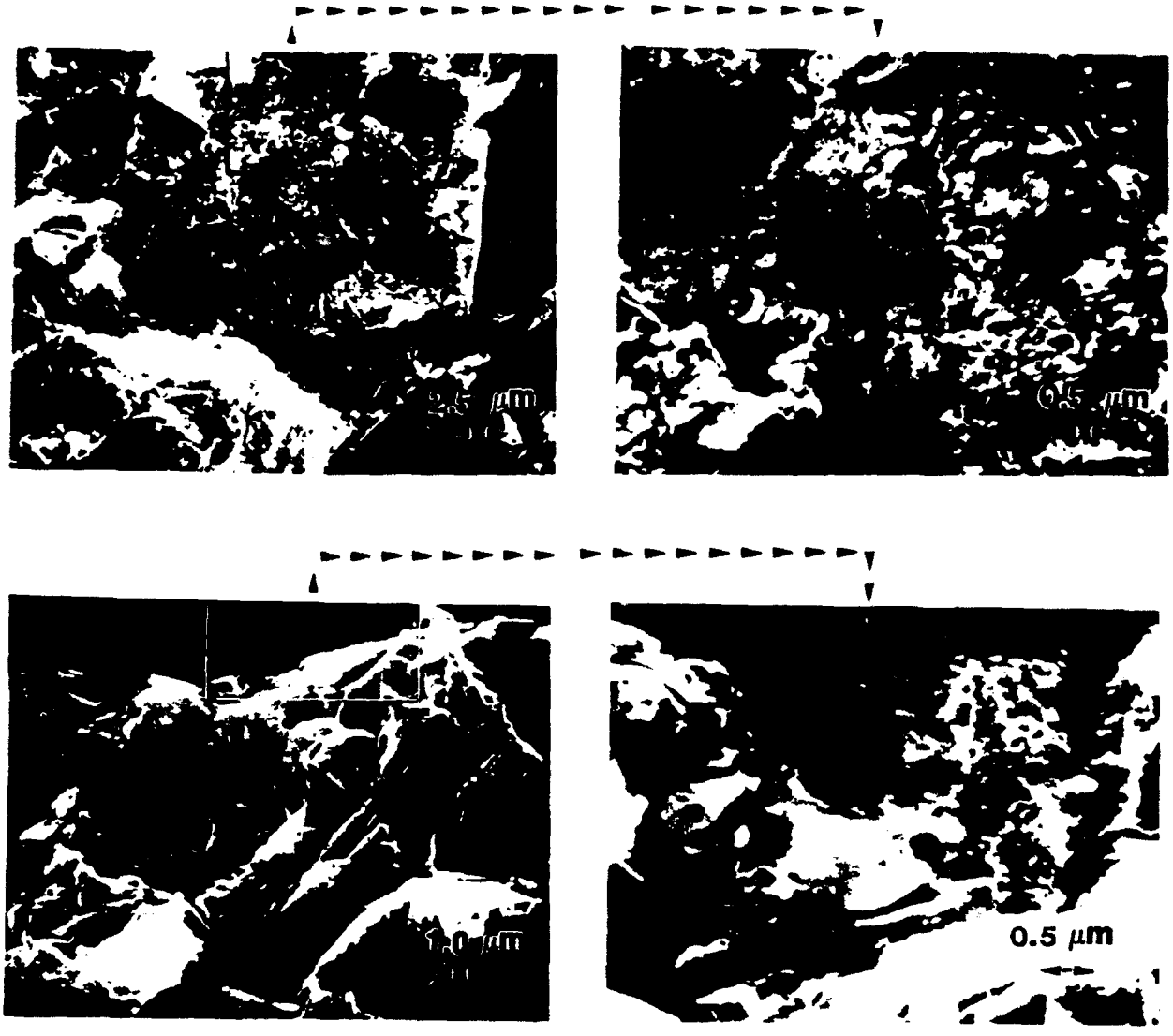

Sample 9213-06, Warren GE SYN # 927H-9 & 101H-4, 8h 800°C Ar, Impact Velocity 1.85 km/s, Fracture Surface

Fig. 26. SEM images from a fracture surface of compact # 9213-06, showing evidence of deformation structure, fine hair-line microcracking, and possible phase separation in particle interiors.

4.2 X-ray Diffraction Analysis

The shock consolidated diamond compacts were analyzed via x-ray diffraction (XRD) analysis to determine the presence of any non-diamond phases. XRD analysis was performed on both the impact and non-impact faces of the compacts. Additionally, the diamond powders were also characterized by XRD, in the as-received as well as in the heat-treated state. In general, although the x-ray detection capability is limited to 10%, by employing slow speed scans and controlled parameters, the detection limits can be improved to at least qualitatively determine the presence of minor phases.

Figure 27, 28, and 29, show typical XRD traces of diamond powders and corresponding compacts for DAC DeBeers natural 1-8 μm, DAC DeBeers synthetic 1-8 μm, and Warren GE synthetic 2-8 μm diamond. The following observations can be made by carefully comparing the XRD traces of the powders and compacts:

(a) An 8 hour 800° C heat treatment in Ar atmosphere yields no difference in powder characteristics as shown in XRD trace.
(b) The shocked compacts show minor peaks at ~30° and ~60° two-theta angles, in addition to those of pure diamond.
(c) The shocked compacts show considerable peak broadening as well as shifts in the d-spacing of the diamond peaks.

The extraneous minor peaks in the XRD traces of compacts indicate presence of minor amounts (< 5%) of graphite. The (111) XRD peak broadening and shifting evident in the compacts, and shown more clearly in figure 30 for (a) DAC natural and (b) DAC synthetic compacts is attributed to presence of defects forming due to plastic deformation of diamond powders during consolidation. Typical shifts in d-spacings are: from 2.0590 A for Warren GE synthetic powder to 2.0557 A for compact; from 2.0585 A for DAC synthetic powder to 2.0616 A for compact; and from 2.0596 A for the DAC natural powder to 2.0694 A for compact.

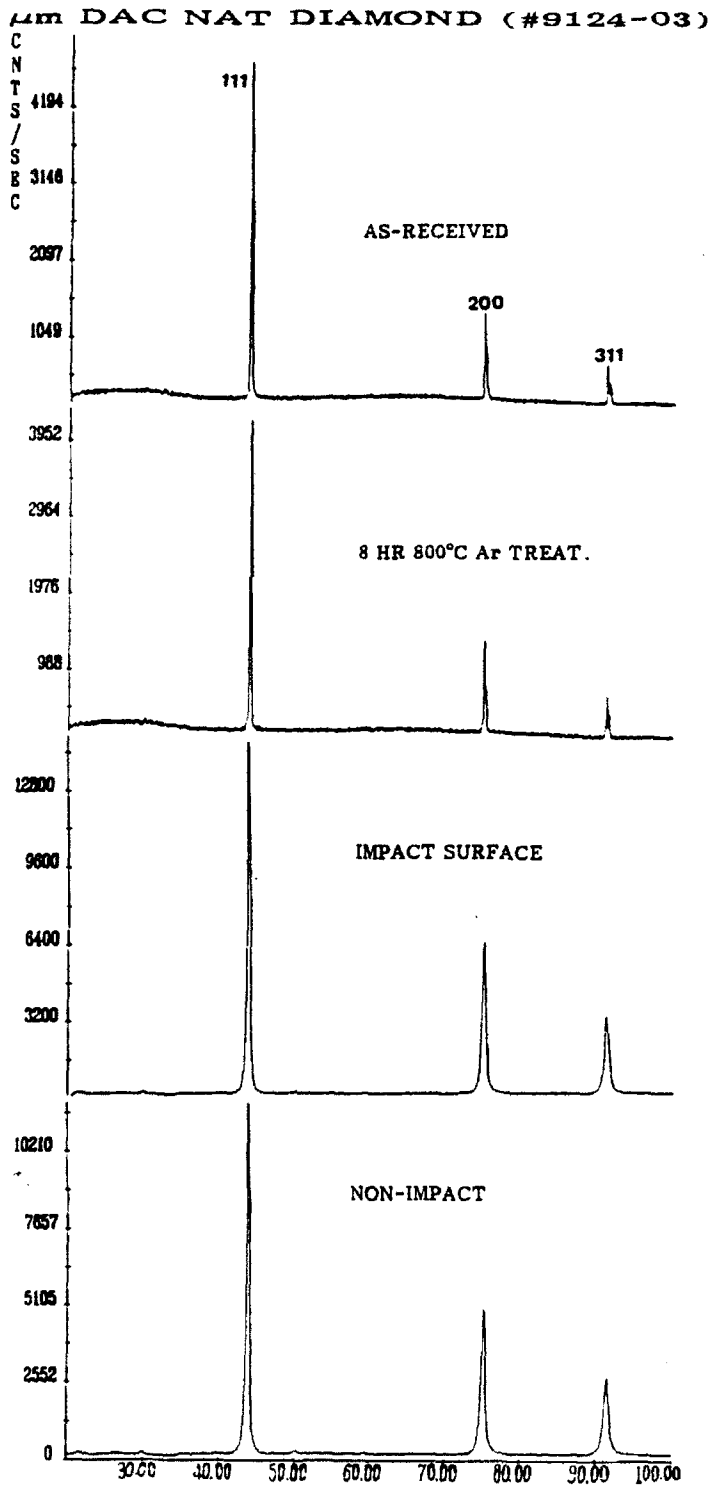

Fig. 27. Typical XRD traces of DAC natural powder in (a) as-received and (b) 8 hour Ar treated state, and of (c) impact and (d) non-impact surfaces of compact # 9124-03

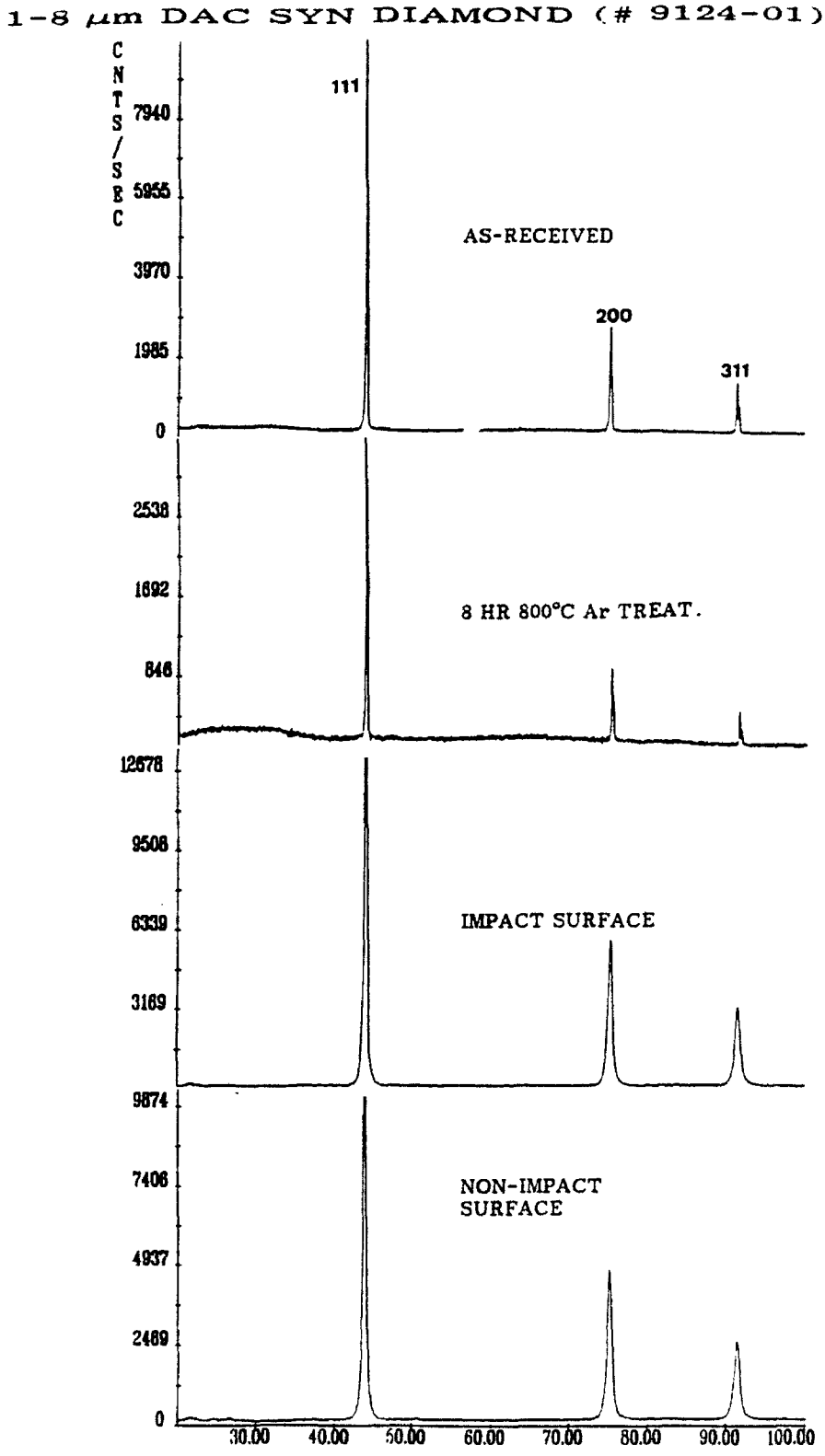

Fig. 28. Typical XRD traces of DAC synthetic powder in (a) as-received and (b) 8 hour Ar treated state, and of (c) impact and (d) non-impact surfaces of compact # 9124-01

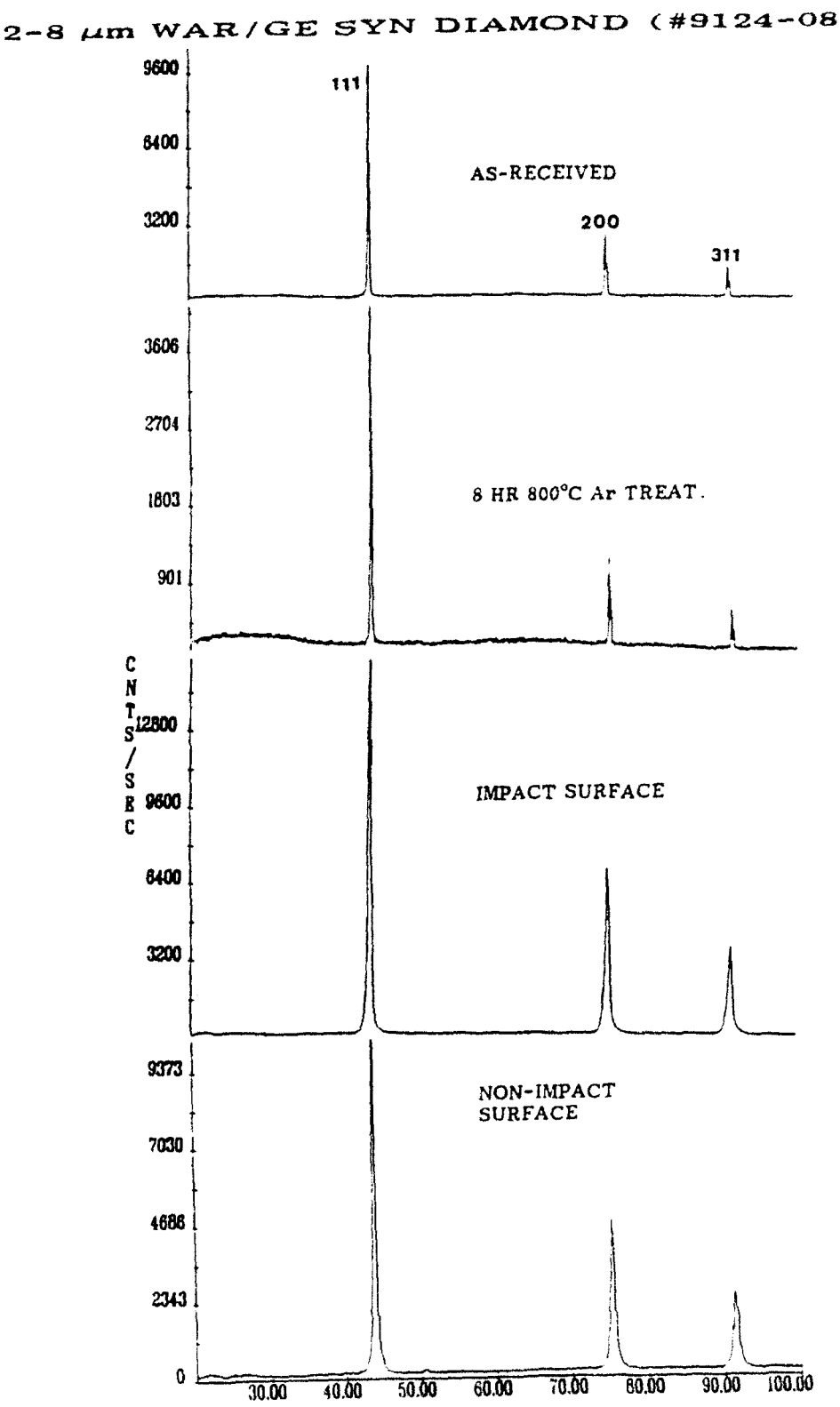

Fig. 29. Typical XRD traces of Warren GE synthetic powder in (a) as-received and (b) 8 hour Ar treated state, and of (c) impact and (d) non-impact surfaces of compact # 9124-08

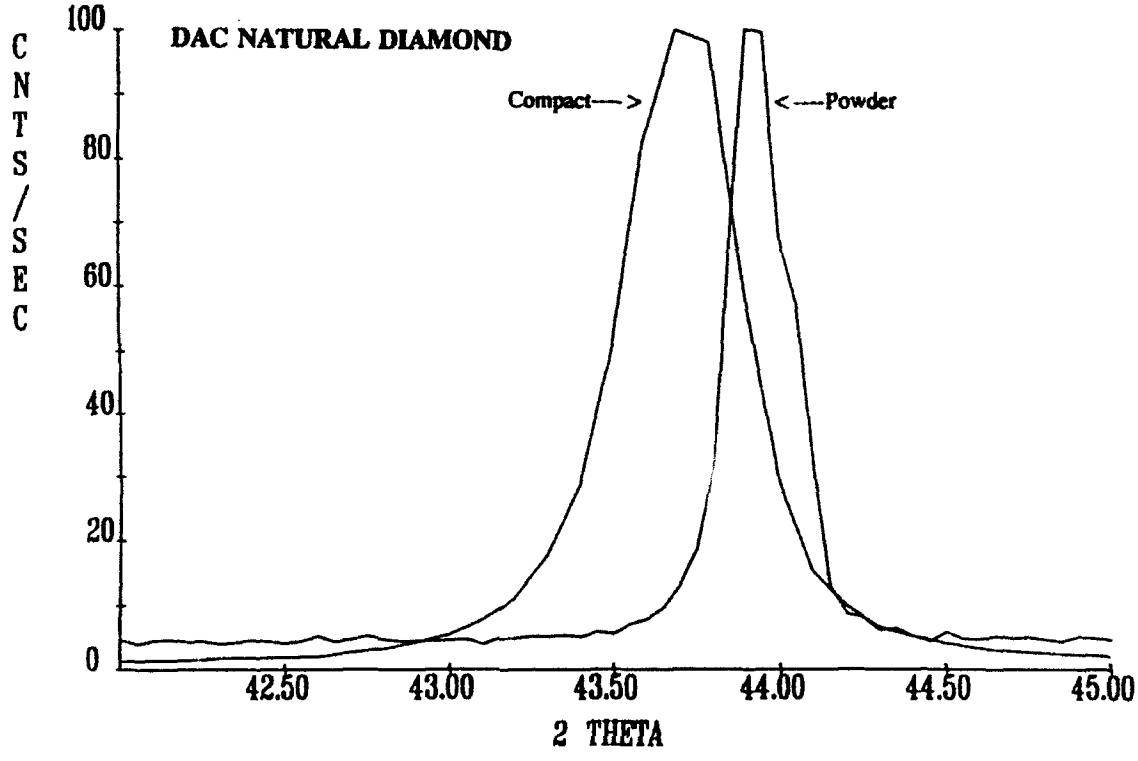

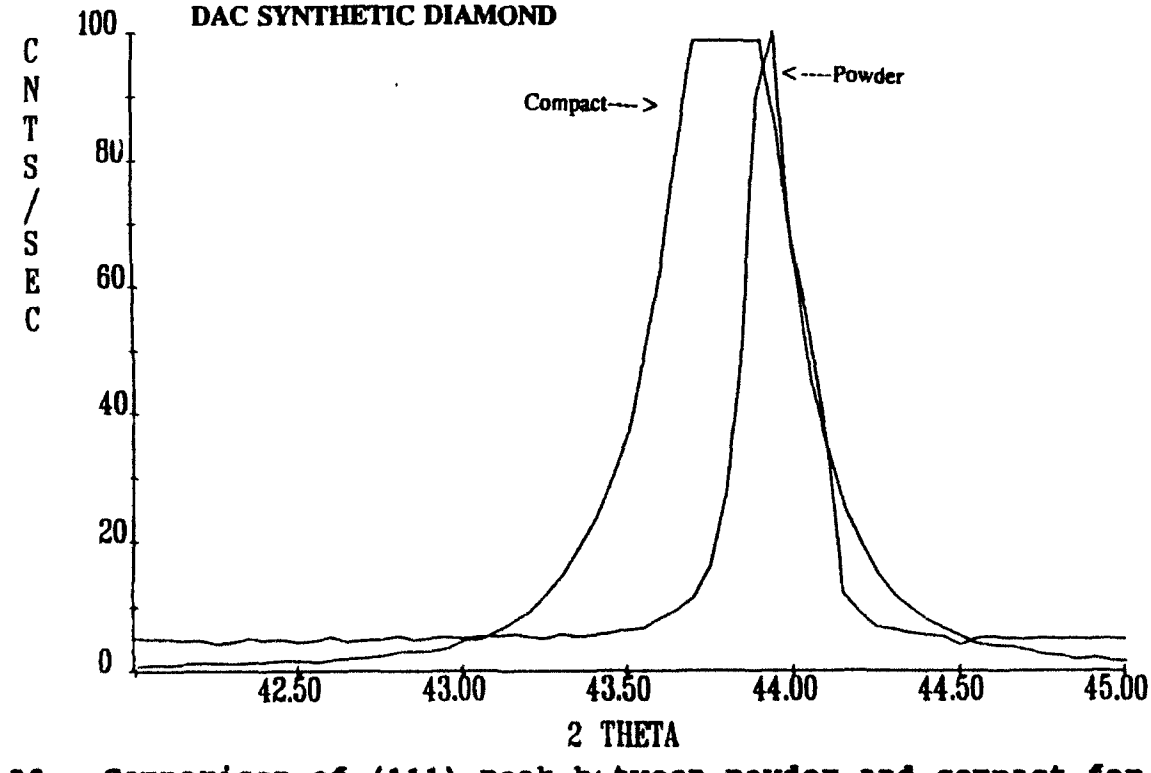

Fig. 30. Comparison of (111) peak between powder and compact for (a) DAC natural and (b) DAC synthetic diamond.

4.3 Raman Spectroscopy Analysis

Accurate determination of graphite and/or amorphous carbon formation was obtained by Raman spectroscopy performed at Allied-Signal. In general, compacts with lower final compact densities, made from powders packed at lower initial densities, showed graphite formation. Raman spectra comparing traces for diamond powder and impact and cross-sectional surfaces of compact # 9201-01 are shown in Fig. 31. While the as-received powder has a sharp diamond peak at 1332 cm^{-1} scattering, the compacts show broader diamond peaks as well as peaks of graphite at 1602 cm^{-1}. The peak broadening is indicative of residual stresses introduced due to excessive plastic deformation during shock compaction.

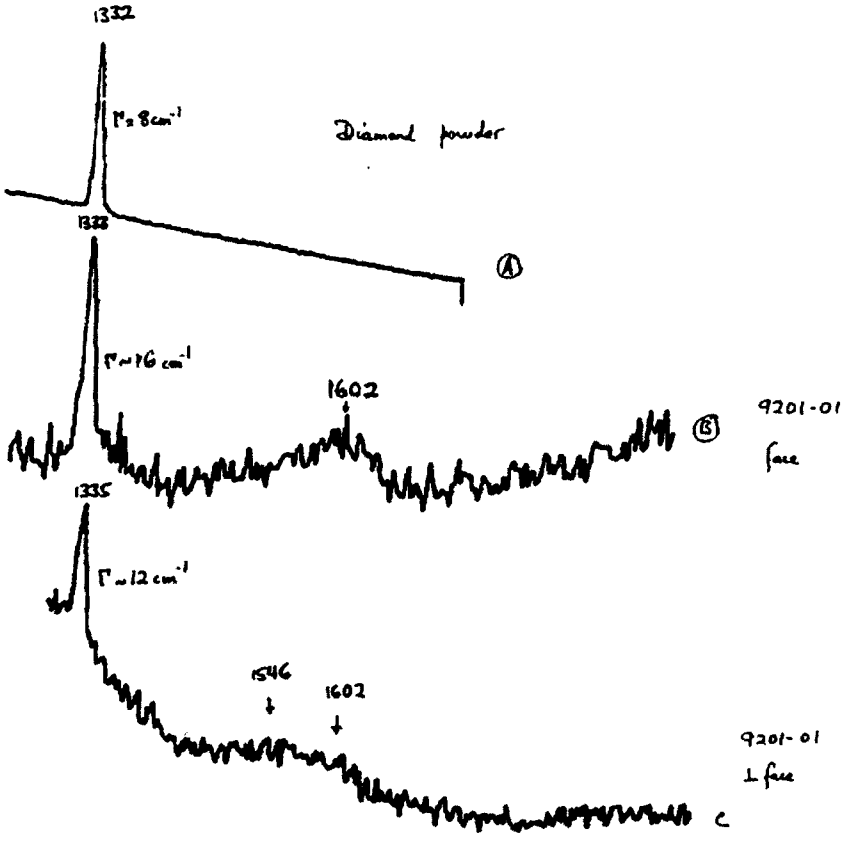

Fig. 31. Raman spectra comparing traces for (a) diamond powder, linewidth Γ = 8 cm^{-1}, (b) impact surface of compact # 9201-01 (Γ = 16 cm^{-1}), graphite line centered at 1602 cm^{-1}, (c) cross-sectional surface of compact 9201-01, (Γ = 12 cm^{-1} and possible amorphous carbon at 1546 cm^{-1}.

The formation of graphite at particle interfaces varies in content and type from the impact surface to inside the compact and from the outer compact edge to the center. Figure 32 compares the Raman spectra at the center and edge regions of compact # 9240-01, and Figure 33 compares the Raman spectra at the center and edge regions of compacts # 9240-03 and 9240-07.

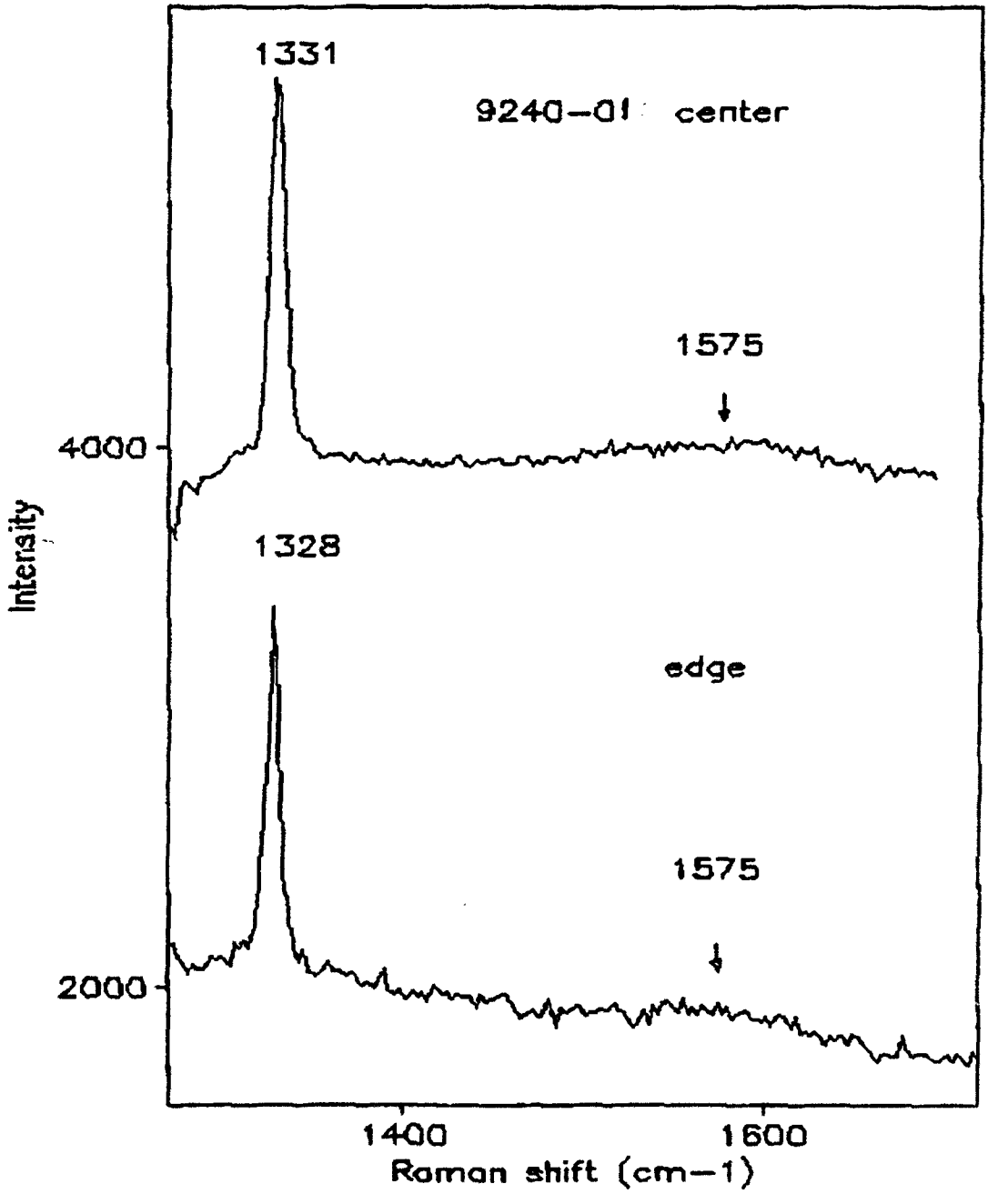

Fig. 32. Comparison of Raman spectra at the center and edge regions of compact # 9240-01.

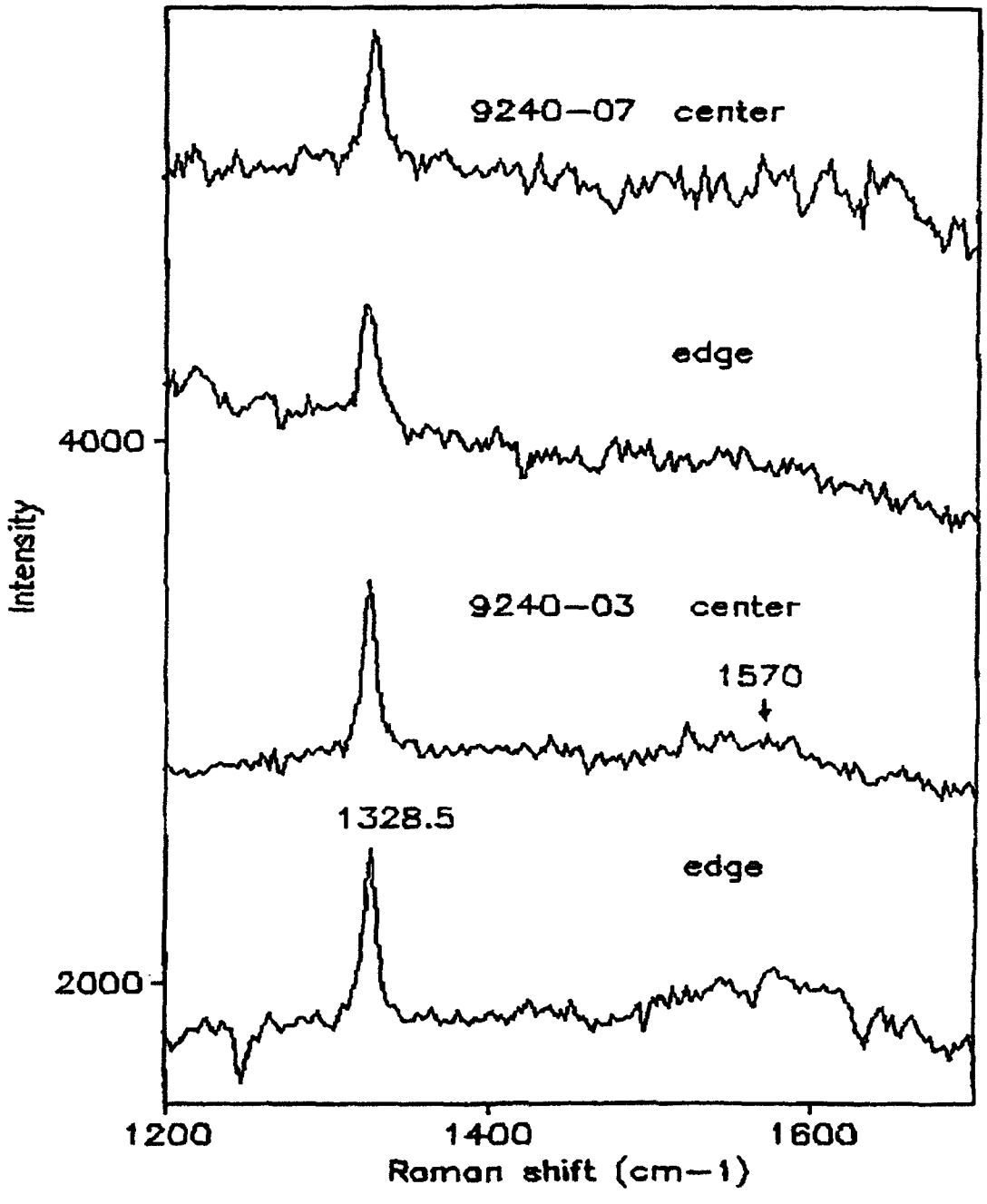

Fig. 33. Comparison of Raman spectra at the center and edge regions of compacts # 9240-03 and 9240-07.

CHAP. 5 - THERMAL CONDUCTIVITY MEASUREMENTS AND RESULTS

The initial thermal conductivity measurements were performed, at CalTech, on the shock consolidated diamond compacts by correlating the ultrasonic velocity with the thermal conductivity based on the Debye approximation. Thus, by measuring an average phonon velocity for the shocked compacts and comparing it with that of single crystal diamond, an approximate estimate of the thermal conductivity of the diamond compact can be extrapolated.

A more direct thermal conductivity measurement employing the laser pulsed photometry technique was also performed at Caltech. Details of both the indirect and direct thermal conductivity measurements will be provided in the following subsections.

5.1 Ultrasonic velocity and thermal conductivity:

The Debye formula for the thermal conductivity of dielectric solids gives,

$$K = \frac{1}{2} C_p \bar{v} \ell \qquad (6)$$

where, K is thermal conductivity, C_p is specific heat, v is mean phonon velocity, and l is the mean Umklapp phonon scattering distance. When a polycrystalline sample's thermal conductivity is limited by phonon interaction at crystallite boundaries, due to cracks and initial crystal dimensions, it can be assumed that the effective phonon velocity is decreased, as the Umklapp distance, l and C_p, are to first order insensitive to grain boundaries.

Thus, based on the assumption that for polycrystalline shock compacted diamond with microcracks,

$$K \propto \bar{v} \qquad (7)$$

we measured the ultrasonic compressional velocity (V_p) and shear velocity (V_s) using the ultrasonic apparatus at CalTech. The

values obtained are:

$$V_p = 4.13 \pm 0.18 mm/\mu sec$$

$$V_s = 3.60 \pm 0.06 mm/\mu sec$$

By averaging the longitudinal and shear phonon modes, these give a mean effective phonon velocity,

$$\overline{v} = 3.86 mm/\mu sec$$

In comparison, for single crystal diamond, using McSkimin's[26] data for the single crystal and calculated Hashin Shtrickman bounds we calculate a mean phonon velocity of:

$$\overline{v} = 13.79 mm/\mu sec$$

Thus, correlating the measured mean phonon velocity for the diamond compact with the calculated single crystal value[27], we infer that the shock consolidated diamond is expected to have a room temperature thermal conductivity 0.28 times the single crystal value.

5.2 Laser Pulsed Photothermal Radiometry

The laser pulsed photothermal radiometry technique is a quick, convenient, non-destructive measurement method. In the present work, analyses using a one-dimensional thermal diffusion model were compared with experimental data. Measurements of the thermal conductivity of a molybdenum foil and several shock-consolidated samples were executed.

Theoretical Considerations: An analytical model describing one-dimensional heat flow was developed to reduce the measured signal to a thermal conductivity for the sample. For a thin sample (thickness<<width), if heat flux is given to the front surface at t=0 as a delta function and there is no heat loss to air at either surface, the temperature rise at the back surface

of the sample is given by:

$$\frac{\Delta T(t)}{\Delta T(\infty)} = \frac{4}{\sqrt{t^*\pi}} \sum_{n=o}^{\infty} exp[-(2n+1)^2/t^*] \qquad (8)$$

where $t^* = 4\alpha t/L^2$, L is the thickness, α is the thermal diffusivity and t is time. Thermal conductivity k is determined by $k=\rho\alpha c$ where ρ is the density and c is the specific heat. The non-dimensional temperature rise due to a transient heating pulse was calculated and is shown in Figure 34.

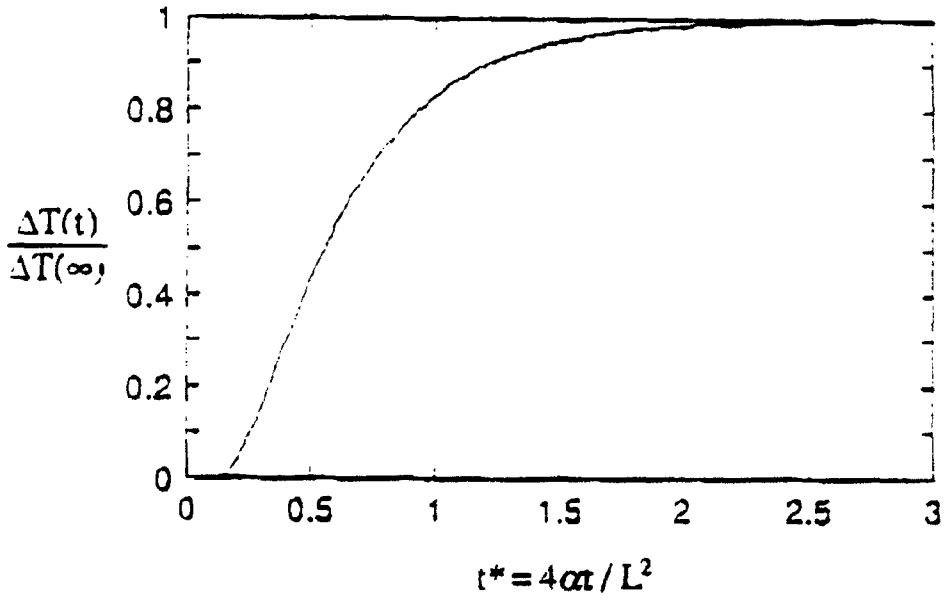

Fig. 34. The calculated non-dimensional temperature rise due to a transient heating pulse

Experimental Technique: Our basic experimental set up is shown in Figure 35. The front of the sample was heated by a pulsed Nd:YAG laser beam. Infrared radiation from the back surface of the sample was focused onto a HgCdTe infrared detector. The detector monitored the rise in temperature as heat propagated from the front surface to the back surface. The resistance of the detector is changed proportional to the incident infrared radiation and by this signal we can get the temperature-time history of the back surface. The back surface of the sample was coated with a black paint whose emissivity was assumed to be unit. Noise during excitation pulse was suppressed by using a gated integrator, acquiring one point per laser pulse. The signal-to-noise ratio of the measurement was improved greatly by use of a germanium filter directly over the detector element to exclude scattered laser light.

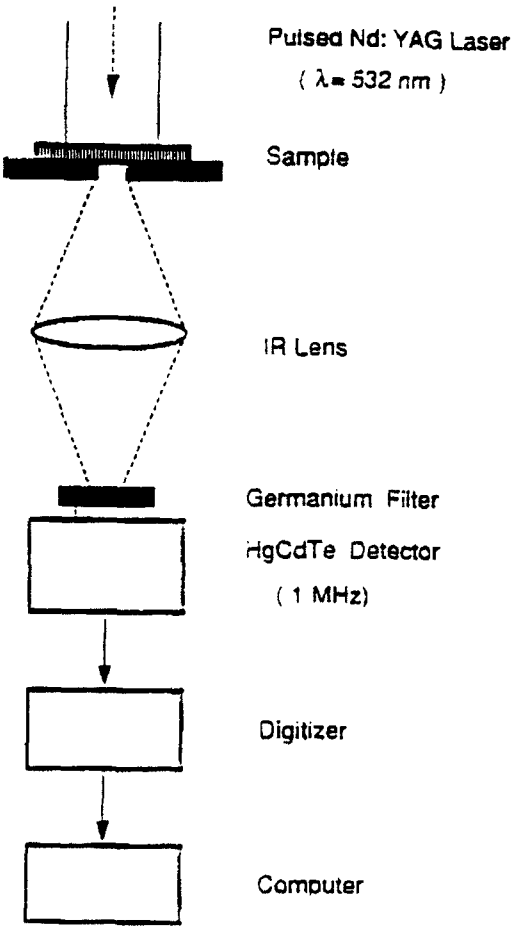

Fig. 35. Experimental set up for pulsed photo radiometry for thermal conductivity measurements.

Experimental Results: Experiments were made for a molybdenum foil and several shock-consolidated diamond samples. Typical signals obtained from a molybdenum foil are shown in Figure 35 (a). The peak at short times is due to residual stray light. This is followed by a rise due to the increasing infrared radiation detected from the back of the foil. The slight decreasing of the signal above times of 300 μs is due to heat loss to the air. The thickness of this foil was 135 μm. Using this value along with typical handbook values for the density and specific heat for molybdenum at 300 K, thermal conductivity was calculated. Theoretically, any value of t* should give the same thermal conductivity. Since experimental results show some deviation from the theoretical temperature rise curve, selecting different values of t* results in different values of thermal conductivity. For a one-dimensional solution, if we choose t*=1 as a reference non-dimensional time scale, α is given by $L^2/4t$. Since the non-dimensional temperature rise $\Delta T(t)/\Delta T(\infty)$ corresponding to t*=1 is 0.83, we can calculate the α by determining the t* which corresponds to this value.

Typical literature values for molybdenum foil at 300K are ρ=10240 kg/m^3, c=255 J/kgK and k=1.39 W/cmK. The experimental value of k with t*=1 was 1.12 W/cmK. This value is 24% lower than the handbook value. Since errors are mainly generated at the early stage of the signal, we can significantly reduce the error by choosing relatively a high value of t*. Selecting $\Delta T(t)/\Delta T(\infty)$=0.99, the experimental value of k is 1.31 W/cmK, which is 6% lower than the handbook value. The results for a molybdenum foil are: thickness = 135μm, literature k at 300K = 1.39 W/cmK, $\Delta T(t)/\Delta T(\infty)$ = 0.83 (or 0.99), experimental k = 1.12 (or 1.31) W/cmK, error = 24% (or 6%).

Thermal conductivities for some shock-consolidated diamond samples were measured and calculated similarly. A typical signal obtained from a shock-consolidated diamond sample is shown in Figure 36 (b) and for a CVD sample is shown in Figure 36 (c).

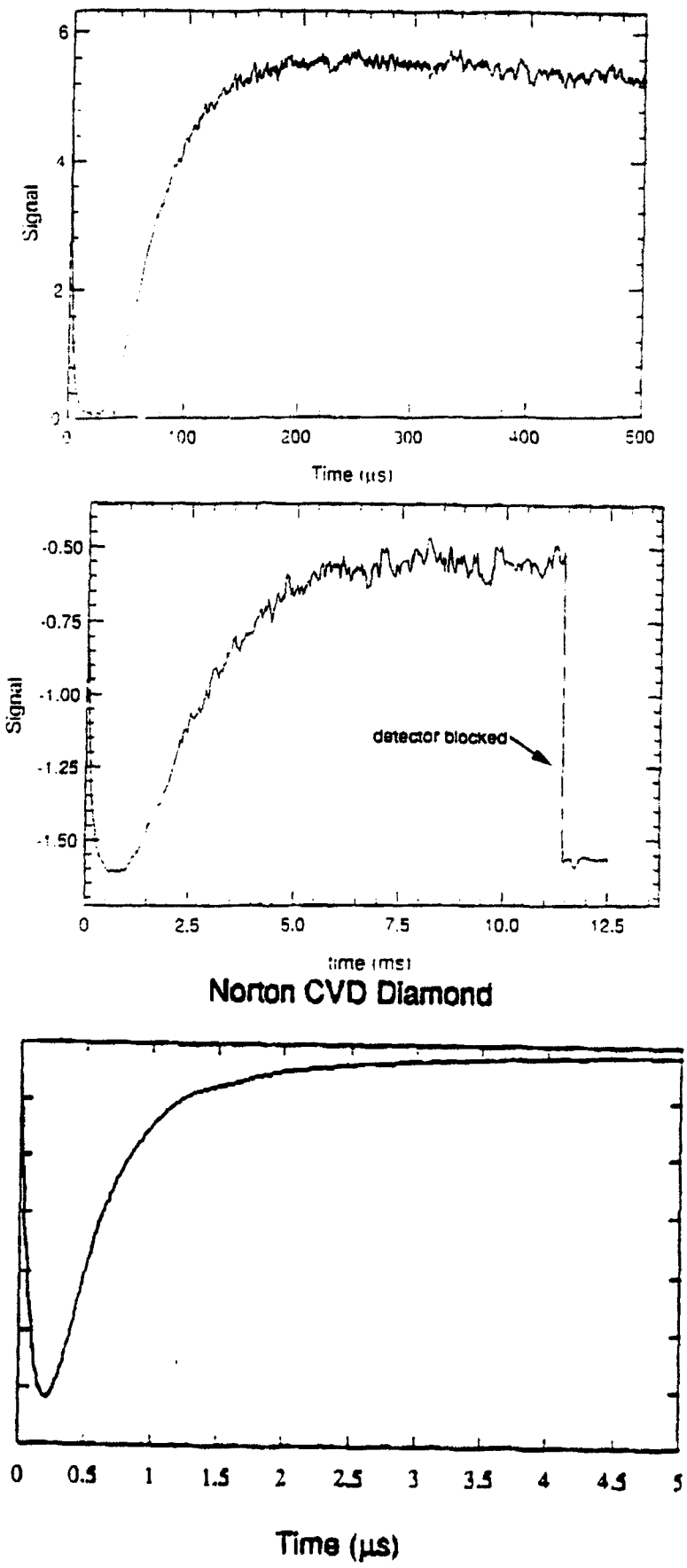

Fig. 36. Measured detector signals for (a) molybdenum foil, (b) shock compacted diamond, and (c) Norton's CVD diamond.

For diamond, the handbook density and specific heat values at 300 K are ρ=3515 kg/m^3, c=516 J/kgK. Thermal conductivity for diamond is dependent on its type and can be as high as 21 W/cmK. The experimental data for shock-consolidated diamond samples are tabulated in Table V.

The density (%) is the measured density, compared with the theoretical density of diamond, ρ=3515 kg/m^3. The results show that these shock-consolidated samples have anomalously low thermal conductivities. The detected signal for one calibrated CVD diamond sample donated by Norton company is shown in Figure 28 (c). The very rapid appearance of the thermal signal on the back surface is evidence of the sample's high thermal conductivity. The rise time is comparable with the detector response time, making it difficult to determine the actual thermal conductivity of this sample.

TABLE V - EXPERIMENTAL DATA OF THERMAL CONDUCTIVITY MEASUREMENTS

Sample #	Diamond type & Density	Thickness	$\Delta T(t)/\Delta T(\infty)$	Diffus. (cm^2/s)	Conduct. (W/cm/K)
9201-02	DAC Syn 9225, 2-8μm (94.5%) (1 hr, 800°C oxidation)	0.670 mm	0.83 0.99	0.106 0.138	0.171 0.220
9201-03	DAC Nat 9226, 2-8 μm (93.3%) (8 hr, 800°C Ar flow)	0.428 mm	0.83 0.99	0.096 0.123	0.168 0.209
9201-05	Warren/GE 300S, 101H-4 (92%) (8 hr, 800°C, Ar flow)	0.575 mm	0.83 0.99	0.112 0.169	0.187 0.282
9201-07	Warren/GE 300S (93.3%) 927H-9 (70%) + 101H-4 (30%) (8 hr, 800°C, Ar flow)	0.442 mm	0.83 0.99	0.095 0.098	0.160 0.166
9201-09	DAC Nat 9226 + 5% Cu (94%) (8 hr, 800°C, Ar flow)	0.588 mm	0.83 0.99	0.09 0.118	0.169 0.201
9124-04	DAC Nat 9226/1 (95.9%) (1 hr, 800°C oxidation)	0.423 mm	0.83 0.99	0.101 0.119	0.164 0.191
9131-10*	Warren/GE 300S, 927H-9	1.060 mm	0.83 0.99	0.208 0.295	0.327 0.465

*Fractured Sample

CHAP. 6 - DISCUSSION OF COMPACTION CRITERION AND MECHANISMS

The consolidation of powders during shock compaction occurs due to the preferential deposition of shock energy at inter-particle regions, which results in extensive plastic deformation and/or friction localized at particle surfaces. While the shock energy is basically generated due to the collapse of voids, the localization of plastic deformation and/or friction can produce extensive heating of the particle near-surface material. Generally, for most metallic and ceramic materials, heat equilibration between the ~1 μm thick particle surface layer and the bulk (interior) of a 10 μm diameter particle (assuming spherical geometry) occurs in time scales of several microseconds.[28] In such a situation, the high temperature retained at the surface layer can result in melting and fusion of particles in contact with each other. In certain cases, particle fusion and solid-state bonding is also possible at temperatures below the melt temperature.[18] In fact excessive heat localization and therefore formation of an excess melt fraction can lead to (a) generation of voids in the last material to solidify from the liquid, (b) formation of large grained microstructures, (c) reversal transformation of metastable phases to equilibrium structures, as well as (d) creation of excessive residual thermal stresses that can lead to microcrack formation.[18]

Diamond is a material that behaves very differently from most materials, because of its very high hardness and thermal conductivity and also because of the possible diamond-to-graphite phase reversal transformation. High hardness implies that significantly higher pressures are required to introduce plastic deformation due to compression of the particles and/or interparticle friction. The high thermal conductivity of diamond limits the retention of heat over time scales sufficient to attain good interparticle bonding. Conversely, longer heat retention causes diamond to transform to the graphitic structure.

The experimental work performed in the present study, involved the use of different variations of powder particle morphologies and surface treatments (and coatings), to overcome the problem of rapid heat conduction and resulting lack of heat retention at localized particle interfaces. On the other hand, initial packing densities of the powders prior to shock consolidation were controlled to minimize long thermal excursions.

A numerical calculation was also performed to estimate the cooling characteristics of the diamond compacts during consolidation. Considering a 10 μm diamond powder particle at room temperature, and a 1 μm thick surface (shell) layer at a temperature of 4850 K generated due to preferential deposition of the shock energy, the times for attaining temperature equilibration were determined, using simple heat transfer calculations.

The flow of heat in a sphere, when the initial and surface conditions are such that isothermal surfaces are concentric spheres and the temperature thus depends only upon the coordinates r and t, is given by Carslaw and Jaeger[29]

$$\frac{\partial v}{\partial t} = \kappa\left(\frac{\partial^2 v}{\partial r^2} + \frac{2\partial v}{r\partial t}\right)$$

where v is the heat flux, t is the time and r is the radius. This can be converted for numerical analysis by setting

$$\Delta T = \alpha .\ \Delta t\left(\frac{\partial^2 T}{\partial r^2} + \frac{2\partial T}{r\partial t}\right)$$

where T is the temperature, and $\alpha = \kappa/\rho c$. The 1st partial derivative for nth node can be calculated as:

$$\frac{\partial T}{\partial r} = \left(\frac{T_{n+1} - T_{n-1}}{2\ \Delta r}\right)$$

and similarly, the 2nd derivative (partial) as:

$$\frac{\partial^2 T}{\partial^2 r} = -\left(\frac{-T_{n-1}+2T_n-T_{n+1}}{2\,\Delta r^2}\right)$$

Substituting these two, we get

$$\Delta T = \alpha\Delta t\left(\frac{T_{n-1}-2T_n+T_{n+1}}{2\,\Delta r^2}+\frac{2}{r_n}\;\frac{T_{n+1}-T_{n-1}}{2\Delta r}\right)$$

for nth node.

Introducing boundary conditions, and having large number of nodes, the temperature at nth node in prior time step shifts to n+1 th node in current time step. This generates a condition when total heat content remains constant and heat transfer is a non-steady state process (transient). Assuming a nominal value of thermal conductivity (κ) of diamond to be 21 W/cmK and specific heat (C) to be 516 J/kgK, we obtain α ($=\kappa/\rho C$) as 1.1×10^{-4}. Substituting for core temperature (298K) and surface temperature (4850K) as initial conditions, the temperature profiles are obtained for various times and are plotted in Figure 36 (a).

It can be seen in Fig. 37(a) that temperature equilibration between surface layer and interior of particle is reached extremely fast, in ≈100 ns. The surface layer would thus, never be able to form a melt phase or even retain high temperatures for a long enough time to allow interparticle bonds to form.

In another context, if degradation of thermal conductivity materials is taken into consideration, assuming high temperature effects, or due to the presence of metallic or other impurities on surfaces of the diamond powders, then the calculated temperature-time contours show a different form. Figure 37 (b) shows temperature contours for the same 1 μm surface layer (at melt temperature) and 10 μm particle (at ambient condition) configuration, with thermal conductivity value degraded to 650 W/mK.

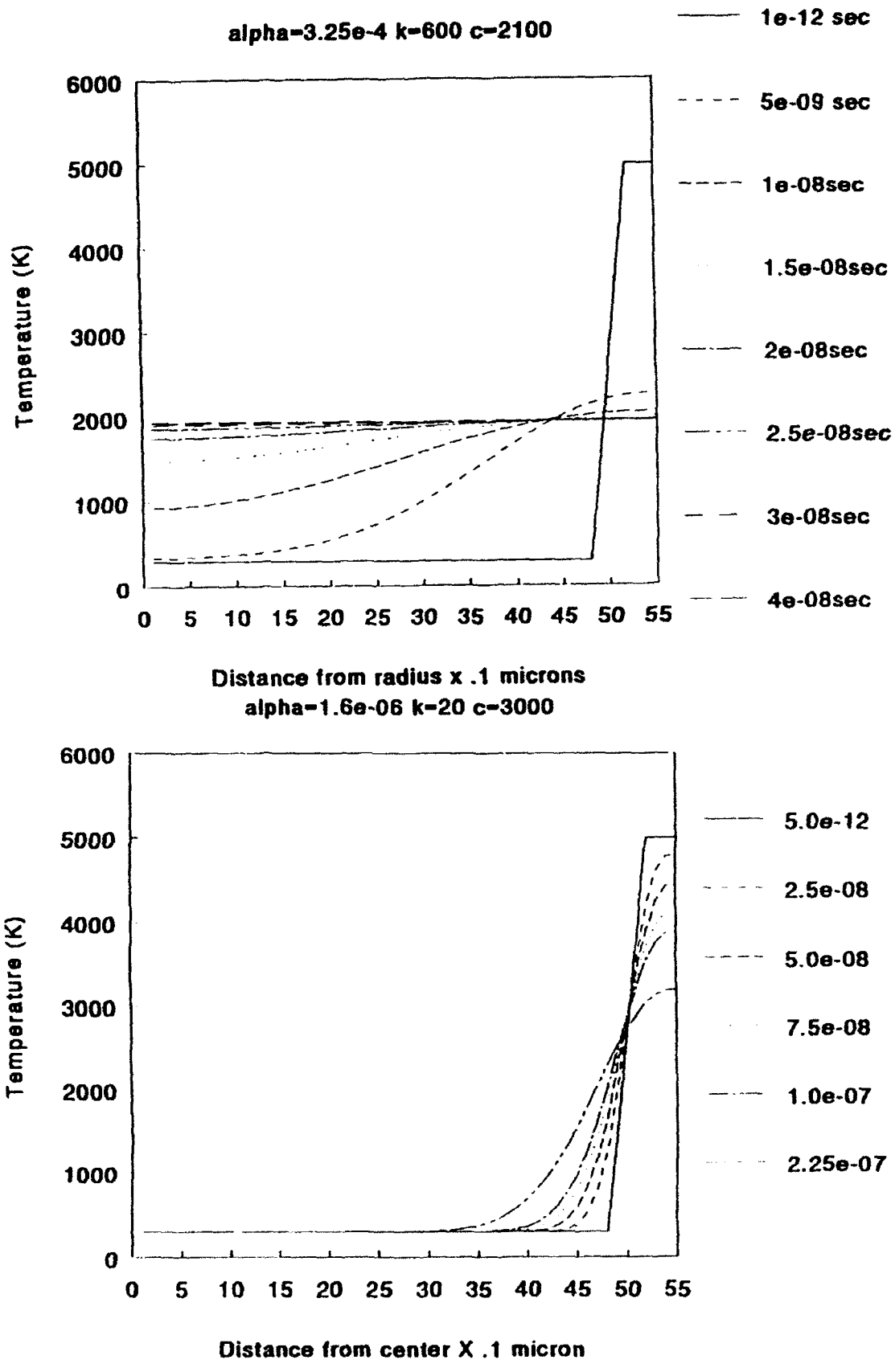

Fig. 37. Temperature contours for cooling of (a) 10 μm pure diamond particle, and (b) contaminated diamond particle with degraded thermal conductivity.

From Fig. 37(b), it can be seen that in a time scale of ~ 2 μs, the temperature rise has reached no more than even a 2 μm thick diamond particle layer. Temperature equilibration between surface layer and bulk of particle would, thus, require more than a few microseconds time scale. Graphitization of diamond can be expected in such cases, if unloading of pressure from the high-pressure to the ambient state is not attained within this time.

The values of degraded thermal conductivity used in the present calculations, are only an estimate, and depend not only on the shock-induced temperature generated at particle surfaces, but also on metallic/organic contaminations on powder surfaces.

We believe that diamond powders acquired in the present study were not contamination-free. They contained known/unknown types of metallic and organic contaminations, and in spite of some of the cleansing treatments used, the powders may not have been fully decontaminated. The SEM micrographs shown in Figures 22-25 are evidence of presence of contaminations that lead to formation of the observed amorphous-like features. Degradation of thermal conductivity, due to presence of these low-conductivity surface contaminations, in addition to its decrease at high temperatures, is attributed to the prolonged retention of elevated temperatures at particle interfaces. Under such conditions, formation of up to 3-5% volume fraction of graphitic and/or amorphous carbon phases at particle interfaces is inevitable. Furthermore, if the graphitic or amorphous carbon phase is particularly present at interparticle bond regions, then the anomalously lower thermal conductivities of the shock-consolidated diamond compacts would be expected.

7. SUMMARY AND CONCLUDING REMARKS

The objectives of the present work were to fabricate 1 mm thick diamond compacts by shock-wave consolidation of powders. In this study, a consolidation criterion of diamond powders of various types (natural and synthetic) and different particle morphologies, treated with different types of surface cleansing and coating processes was studied. The fundamental issues investigated, included establishing the effects of starting powder characteristics and shock consolidation conditions, as well as correlating these effects to compact microstructure and properties, to develop consolidation mechanisms. The following list summarizes the highlights of the present study.

(a) Diamond compacts 12 mm diameter by 1 mm thickness, made from various types of commercially available natural and synthetic diamond powders were consolidated to 90-95% TMD range;

(b) Optimum consolidation conditions were achieved by controlling initial powder packing densities achieved by appropriate selection of powder particle size and size distribution;

(c) Diamond powder surface treatments by thermal annealing or coating were observed to have beneficial effects and helped in better recovery of the compacts;

(d) Final compact densities increased from 70-75% range to 88-95% range with initial packing density change from 60-65% to 70-75%;

(e) The diamond compacts were free from macro-cracks (observable with naked eye), and had strong mechanical integrity;

(f) Increase of shock conditions (> 2 km/s) marginally increased final densities, although compact recovery became difficult.

(g) All diamond compacts contained 3-5% graphitic and/or amorphous carbon phase, the content of which increased with increasing impact velocity and decreasing initial powder-packing-density.

(h) Significant residual strain, indicated by broadening of peaks of Raman spectra and XRD traces, was observed in all compacts;

(i) Thermal conductivities of compacts, measured using Laser Pulsed Photothermal Radiometry, yield anomalously low values;

(j) The low thermal conductivities of the diamond compacts are attributed to the presence of surface contaminations on powder surfaces, 3-5% volume fraction of graphite or amorphous carbon formed during shock compaction, and excess residual strain due to extensive plastic deformation of powders during shock consolidation.

In conclusion, it needs to be emphasized that in the time period the present study was performed many experiments were conducted to explore a wide variety of materials and processing variables. The experiments have also provided a large number of samples, some of which have been analyzed in more detailed than others, and some still remain to be analyzed. The present study has also yielded diamond compacts that are the best of their kind in terms of compact integrity and overall microstructural characteristics.

No data is presently available which directly correlates the effects of residual strain due to the presence of point, line, and planar defects, or the volume fraction of graphite or even porosity, on thermal conductivity. Thus, while problems associated with the process that yield poor overall thermal conductivity can only be speculated with the available results, they need to be targeted with more specific evaluations. Detailed analysis of shock energy localization and heat retention at particle surfaces needs to be performed. Availability of better quality diamond powders and/or cleansing and decontamination treatments, prior to shock consolidation needs to be explored. At the same time, post-compaction techniques for decontamination of non-diamond phases, and annealing of defects, also need to be developed.

It can also be concluded that the time available in the present work was too limited to allow targeted evaluations and in-depth diagnostics, calculations, observations, and measurements. Without such careful evaluation and understanding, and correlations of experimental results with compact microstructures and properties, the complete scope of a process may be difficult to infer. Diamond is a unique material system, and because of its high thermal conductivity, electrical resistivity, high hardness, it not only becomes the material of choice for high electronic substrate applications, but it also is the best model material for the study of dynamic high-pressure shock-compression of powders.

REFERENCES

1. J.E. Fields, The Properties of Diamond, Academic Press, 1979.
2. "Status and Applications of Diamond and Diamond-like Materials: An Emerging Technology", NRC, NAP Washington, 1990).
3. R.C. DeVries, Ann. Rev. of Mater. Sci., 17 (1987) 162-187.
4. J.C. Angus and C.C. Hayman, Science, 141 (1988) 913.
5. A.H. Deutchman and R. J. Partyka, Adv. Mater. and Proc., 135 (6) (1989) 29.
6. P.K. Bachmann and R. Messier, Chem. Eng. News, 5 (1989) 24.
7. C.B. Swan, Proc. I.E.E.E., 55 (1987) 1617-1618.
8. W.H. Gourdin, Mat. Sci. and Engineering, 67 (1984) 179-184.
9. R.L. Williamson and R.A. Berry, in Shock Waves in Condensed Matter, ed. Y. Gupta, Plenum, 1986, 341.
10. T.J. Ahrens, D. Kostka, P. Kasiraj, T. Vreeland, Jr., A.W. Hare, F.D. Lemkey, and E.R. Thompson, in Rapid Solidification Processing - Principles and Technology, III, edited by R. Mehrabian, pp. 672-677, National Bureau of Standards, 1983.
11. D.K. Potter and T.J. Ahrens, App. Phys. Letts.,51 (1987)
12. C.A. Brooks, V.R. Howes, & A.R. Parry, Nature, 332 (1988) 139.
13. A.F. Goncharov, I.N. Makarenko, and S.M. Stishov, JETP, 96 (1989), 670-673.
14. K. Kondo and S. Sawai, J. Amer. Cer. Soc., 73 (1990) 1983.
15. K. Hokamoto, S.S. Shang, L.H. Yu and M.A. Meyers, in Shock-Wave and High-Strain-Rate Phenomena in Materials, eds. L.E. Murr, M.A. Meyers, & K.P. Staudhammer, Marcel Dekker, 1990, p. 453.
16. D.K. Potter and T.J. Ahrens, J. Appl. Phys., 63 (1988) 910.
17. H. Tan and T.J. Ahrens, J. Appl. Phys., 67 (1990) 217-224.
18. N.N. Thadhani, Adv. Mat. & Manuf. Proc., 3(4) (1988) 493-550
19. T. Akashi and A.B. Sawaoka, U.S. Pat. 4,655,830, Apr 7, '87.
20. T. Akashi and A.B. Sawaoka, J. Mater. Sci., 21 (1987) 2221.

21. M. Yoshida, K. Tanaka, and S. Fujiwara, "A computational study of a shock collision fixture for high pressure recovery experiments," in Shock Waves in Condensed Matter - 1987, eds. S.C. SChmidt and N.C. Holmes, North-Holland, 1988, p. 399.

22. A. Mutz and T. Vreeland, Jr., "Several Techniques for One-dimensional Strain Consolidation of Multiple Cavities," in source cited in Ref. 15, p. 425.

23. J.E. Kennedy, "Explosive Output for Driving Metal," in *Behavior and Utilization of Explosives in Engineering Design,* L. Davison, J.E. Kennedy, and F. Coffey, eds., New Mexico Section of ASME, Albuquerque, 1972, p. 109.

24. M. Yoshida, "MY1DL-A One Dimensional Langrangian Analysis Code," CETR Report No. A-05-1986, 1986.

25. ..R. Norwood and R.A. Graham, "Numerical Simulation of Peak Shock Pressure and Mean Bulk Temperature of a CETR/SAWAOKA Plate Impact Recovery Fixture Capsule," source cited in Ref 15.

26. H.J. McSkin and W.L. Bond, "Elastic Modulii of Diamond", Phys. Rev., 105 (1957) pp. 116-121.

27. R. Berman, "Thermal Properties," edited by J.E. Field, Academic Press, NY, 1979, pp. 3-22.

28. R.B. Schwarz, P. Kasiraj, T. Vreeland, Jr., and T.J. Ahrens, Acta Metall., 32 (1984) 1243-1252.

29. H.S. Carslaw and J.C. Jaeger, "Conduction of Heat in Solids," Clarendon, Oxford Press, (UK), 1959.

APPENDIX - A

SAMPLE-BY-SAMPLE LISTING

OF

DIAMOND POWDER COMPACTION EXPERIMENTS

NRL/DARPA DIAMOND POWDER COMPACTION EXPT. # 1

(Updated April 23, 1993)

{SHOT # 9114, 12-CAPSULE SYSTEM, 1" PBX 9501, IMPACT VELOCITY = 1.89 (center), 1.90 (1 side), 1.84-1.86 (other side)}

SAMPLE NUMBER	DIAMOND POWDER TYPE/MAKE & CONDITION	PACKING DENSITY	PLANARITY	RECOVERY	FINAL DENS.	COMPACT PROPS.
9114-01	WARREN/GE 300S-01, 711H (as is)	61.55 %	0.0015"	capsule blown	------- no recovery ---------	
9114-02	DAC SYN 9225/1 (as is)	63.58 %	0.0011"	capsule blown	------- no recovery ---------	
9114-03	DAC NAT 9226/1 (as is)	63.6 %	0.0018"	capsule blown	------- no recovery ---------	
9114-04	WARREN, GE 300S-01, 711H (8h, 800°C, flowing Ar)	63.58 %	0.0010	single piece	87.00%	I/ possible graphit
9114-05	DAC SYN 9225/1 (8h, 800°C, flowing Ar)	64.00%	0.0016	single piece	84.52%	I/N clean diamond
9114-06	DAC NAT 9226/1 (8h, 800°C, flowing Ar)	64.59%	0.0015	two half pieces	85.50%	
9114-07	WARREN/GE 300S-01, 711H (as is) in 1 mm th. Ti+C sandwich	64.70%	0.0004	diamond lost TiC laminates		TiC product & Ti+C and diamond reatained
9114-08	DAC SYN 9225/1 (as is) in 1 mm th. Ti+C sandwich	66.84 %	0.0002"	single piece sandwich		
9114-09	DAC NAT 9226/1 (as is) in 1 mm th. Ti+C sandwich	64.17%	0.0009"	TiC imp. side TiC+Dia non-imp side		
9114-10	WARREN/GE 300S-01, 711H (as is) in 1 mm th. Ti+2B sandwich	64.60%	0.0015"	capsule blown	------- no recovery --------	
9114-11	DAC SYN 9225/1 (as is) in 1 mm th. Ti+2B sandwich	62.60 %	0.0010"	one-half + 2 pcs TiB_2 non-imp side reacted		
9114-12	DAC NAT 9226/1 (as is) in 1 mm th. Ti+2B sandwich	61.22%	0.0008"	frag pieces + TiB_2 imp side reacted pc.		TiB_2 + Ti_3B_4 products and Ti + diamond

NOTE: $Ti + C - TiC$, $\Delta H_R = -44$ kcal/mol; $Ti + 2B = TiB_2$, $\Delta H_R = -77$ kcal/mol

NRL/DARPA DIAMOND POWDER COMPACTION EXPT. # 2

{SHOT # 9115, 12-CAP. SYSTEM, 1" PBX 9501, IMPACT VEL = 1.68 (center), 1.83 (1 side), 1.76-1.77 (other sides)}

SAMPLE NUMBER	DIAMOND POWDER TYPE/MAKE & CONDITION	PACKING DENSITY	PLANARITY	RECOVERY	FINAL DENS./COMPACT PROPS.	
9115-01	WARREN/GE 300S-01, 711H (as is) in 1 mm th. Al_2O_3 sandwich	61.30 %		laminated sandwich		
9115-02	DAC SYN 9225/1 (as is) in 1 mm th. Al_2O_3 sandwich	61.32 %		fragmented pieces		
9115-03	DAC NAT 9226/1 (as is) in 1 mm th. Al_2O_3 sandwich	58.66 %		single pc sandwich		
9115-04	WARREN/GE 300S-01, 711H (as is) in 1 mm th. W sandwich	64.44 %		fragmented sandwich		
9115-05	DAC SYN 9225/1 (as is) in 1 mm th. W sandwich	62.70 %		sandwich fragmented		
9115-06	DAC NAT 9226/1 (as is) in 1 mm th. W sandwich	63.70 %		one piece with cracks		
9115-07	WARREN/GE 300S-01, 711H (as is)	55.00 %		three quadrants		
9115-08	DAC SYN 9225/1 (as is)	55.00 %		one piece		I/ clean diamond
9115-09	DAC NAT 9226/1 (as is)	59.77 %		one piece	72.73%	I/N clean diamond
9115-10	WARREN/GE 300S-01, 711H (as is)	73.20 %		one piece		Raman/cleanest dia spectra+graph+a-C
9115-11	DAC SYN 9225/1 (as is)	61.60 %		one piece		Raman/ graph + a-C
9115-12	DAC NAT 9226/1 (as is)	60.50%		cup and cone pieces		Raman/ least a-C XRD/ clean diamond

NOTE: Al_2O_3 and W powders of approximately -325 mesh size.

NRL/DARPA DIAMOND POWDER COMPACTION EXPT. # 3

(SHOT # 9124, 12-CAPSULE SYSTEM, 1" PBX 9501, IMPACT VELOCITY = 1.9 (center)

SAMPLE NUMBER	DIAMOND POWDER TYPE/MAKE & CONDITION	PACKING DENSITY	PLANARITY	RECOVERY	FINAL DENS./COMPACT PROPS.
9124-01	DAC SYN 9225/1 (8h, 800°C, flowing Ar)	64.20 %	0.0011	single piece	88.6% I/ clean diamond N/ trace graph (?)
9124-02	DAC SYN 9225/1 (1h, 800°C, air oxidation)	59.80 %	0.0014	single piece	86.4% I/N clean diamond with trace grap(?)
9124-03	DAC NAT 9226/1 (8h, 800°C, flowing Ar)	67.60 %	0.0014	single piece	89.7% I/N clean diamond Thermal Cond same as GE CVD diamond
9124-04	DAC NAT 9226/1 (1h, 800°C, air oxidation)	70.45 %	0.0015	single piece	83.05% I/N clean diamond
9124-05	DAC SYN 9225/1 (5h, 200°C, bake 100 μm vac)	65.99 %	0.0015	single piece	92.1% Raman/ amorphous C I/ edge-1338, cen-1335 N/ edge-1337, cen-1339
9124-06	DAC NAT 9226/1 (5h, 200°C, bake 100 μm vac)	69.60 %	0.0011	one half piece	83.95% I/N clean diamond Thermal Cond less than GE CVD diamond
9124-07	WARREN/GE 300S-01, 101H-4 (8h, 800°C, flowing Ar)	70.85 %	0.0020 w/ .0135"sleeve	four quadrants	89.61%
9124-08	WARREN/GE 300S-01, 101H-5 (8h, 800°C, flowing Ar)	66.30 %	0.0010	single piece	85.35% I/N clean diamond
9124-09	DAC SYN 9225/1 + C_{60} coat (8h, 800°C, flowing Ar)	64.80 %	0.0009	single piece	81.4% Raman/ amorphous C I/ edge-1336, cen-1332; N/ edge-1343, cen-1338
9124-10	DAC SYN 9225/1 (8h, 800°C, flowing Ar)	63.60 %	0.0015	cup and cone pieces	87.34% I/N contains graph
9124-11	DAC NAT 9226/1 + C_{60} coat (8h, 800°C, flowing Ar)	67.85 %	0.0007	capsule blown	------- no recovery -------
9124-12	DAC NAT 9226/1 (8h, 800°C, flowing Ar)	67.26%	0.0006	single piece	86.5% I/ clean diamond N/ trace grap (?)

NOTE: C_{60} coating done by dissolving powder in toluene, mixing diamond powder, and evaporating off the solvent.

NRL/DARPA DIAMOND POWDER COMPACTION EXPT. # 4

(SHOT # 9125, 4-CAPSULE SYSTEM, 1" PBX 9501, IMPACT VELOCITY = 1.9 (center)

SAMPLE NUMBER	DIAMOND POWDER TYPE/MAKE & CONDITION	PACKING DENSITY	PLANARITY	RECOVERY	FINAL DENS./COMPACT PROPS.
9125-01	DAC SYN 9225/1 (8h, 800°C, flowing Ar)	61.94 %	UNA	fragments	87.2%
9125-02	DAC NAT 9226/1 (8h, 800°C, flowing Ar)	62.57 %	VAI	fragments	88.2%
9125-03	DAC SYN 9225/1 (5h, 200°C, bake 100 μm vac)	58.89 %	LA	fragments	88.2%
9125-046	DAC NAT 9226/1 (5h, 200°C, bake 100 μm vac)	57.37 %	BLE	fragments	84.8%

NRL/DARPA DIAMOND POWDER COMPACTION EXPT. # 5

{SHOT # 9131, 12-CAPSULE SYSTEM, 1.5" PBX 9501, IMPACT VELOCITY = 2.15 (center)

SAMPLE NUMBER	DIAMOND POWDER TYPE/MAKE & CONDITION	PACKING DENSITY	PLANARITY	RECOVERY	FINAL DENS./COMPACT PROPS.
9131-01	DAC SYN 9225/1 (8h, 800°C, flowing Ar)	63.02 %	U	capsule blown	------ no recovery ----------
9131-02	DAC SYN 9225/1 (5h, 200°C, bake 100 μm vac)	63.02 %	N	capsule blown	------ no recovery ----------
9131-03	DAC SYN 9225/1 + C_{60} coat (8h, 800°C, flowing Ar)	68.17 %	A	capsule broken compact retained	85.22%
9131-04	DAC NAT 9226/1 (8h, 800°C, flowing Ar)	70.0 %	V	two pieces	88.95%
9131-05	DAC NAT 9226/1 (5h, 200°C, bake 100 μm vac)	67.26 %	A	two pieces	93.3%
9131-06	DAC NAT 9226/1 + C_{60} coat (8h, 800°C, flowing Ar)	72.38 %	I	half pc. recovered	
9131-07	WARREN/GE 300S-01, 101H-4 (8h, 800°C, flowing Ar)	66.0 %	L	capsule blown some in edge	-------- no recovery ---------
9131-08	WARREN/GE 300S-01, 101H-4 (5h, 200°C, bake 100 μm vac)	69.26 %	A	capsule blown	-------- no recovery --------
9131-09	WARREN/GE 300S-01, 101H-4 with C_{60} coat (8h, 800°C, flowing Ar)	70.68 %	B	capsule blown	-------- no recovery ---------
9131-10	WARREN/GE 300S-01, 927H-9,100% (8h, 800°C, flowing Ar)	74.02 %	L	two pieces	87.91%
9131-11	WARREN/GE 300S-01, 927H-9(65%) + 101H-4 (35%) (8h, 800°C, flowing Ar)	72.87 %	E	capsule blown	------- no recovery ---------
9131-12	WARREN/GE 300S-01, 927H-9(50%) + 101H-4(50%) (8h, 800°C, flowing Ar)	72.12 %		one half piece	89.22%

NOTE: C_{60} coating done by dissolving powder in toluene, mixing diamond powder, and evaporating off the solvent.

NRL/DARPA DIAMOND POWDER COMPACTION EXPT. # 6

(SHOT # 9132, 4-CAPSULE SYSTEM, 1" PBX 9501, 12" PWL, IMPACT VELOCITY = 1.90 (center)

SAMPLE PROPS. NUMBER	DIAMOND POWDER TYPE/MAKE & CONDITION	PACKING DENSITY	PLANARITY	RECOVERY	FINAL DENS.	COMPACT
9132-01	DAC SYN 9225/1 (8h, 800°C, flowing Ar)	56.38 %	UNA	full piece	79.6%	
9132-02	DAC NAT 9226/1 (8h, 800°C, flowing Ar)	59.5 %	VAI	full piece	88.0%	
9132-03	WARREN/GE 300S, 101H-4 (8h, 800°C, flowing Ar)	56.0 %	LAB	one-half and fragments	90.5%	
9132-04	WARREN/GE 300S, 927H-9 (65%) + 101H-4 (35%) (8h, 800°C, flowing Ar)	63.0 %	LE	four quarters	92.9%	

NRL/DARPA DIAMOND POWDER COMPACTION EXPT. # 7

(SHOT # 9201, 12-CAPSULE SYSTEM, PW80 LENS, 1" PBX 9501, IMPACT VELOCITY = 1.90 (center)

SAMPLE NUMBER	DIAMOND POWDER TYPE/MAKE & CONDITION	PACKING DENSITY	PLANARITY	RECOVERY	FINAL DENS./COMPACT PROPS.
9201-01	DAC SYN 9225/1 (8h, 800°C, flowing Ar)	69.3%			85.88%
9201-02	DAC SYN 9225/1 (1, 800°C, oxidation)	63.6%			89.47%
9201-03	DAC NAT 9226/1 (8h, 800°C, flowing Ar)	72.87%			88.90%
9201-04	DAC NAT 9226/1 (1h, 800°C, oxidation)	67.3%		capsule blown	----- no recovery ----------
9201-05	WARREN/GE 300S-01, 101H-4 (8h, 800°C, flowing Ar)	64.8%			90.04%
9201-06	WARREN/GE 300S-01, 101H-4 (1h, 800°C, oxidation)	69.3%		capsule blown	----- no recovery ----------
9201-07	WARREN/GE 300S-01, 927H-9 (70%) + 101H-4 (30%) (8h, 800°C, flowing Ar)	74.4%			88.76%
9201-08	WARREN/GE 300S-01, 927H-9 (70%) + 101H-4 (30%) (1h, 800°C, oxidation)	72.1%		capsule blown	------ no recovery ----------
9201-09	DAC NAT 9226/1 + 5% Cu (fine) (8h, 800°C, flowing Ar)	67.8%			89.33%
9201-10	WARREN/GE 300S-01 + 10% C_{60} 927H-9 (70%) + 101H-4 (30%) (8h, 800°C, flowing Ar)	72.9%		capsule blown	----- no recovery----------
9201-11	Sodium acetylide	55.87%		capsule blown	----- no recovery ----------
9201-12	Lithium acetylide	52.4%			

NRL/DARPA DIAMOND POWDER COMPACTION EXPT. # 8

(SHOT # 9202, 4-CAPSULE SYSTEM, 1" PBX 9501, 12" PWL, IMPACT VELOCITY = 1.90 (center) 5 mm th. compacts

SAMPLE NUMBER	DIAMOND POWDER TYPE/MAKE & CONDITION	PACKING DENSITY	PLANARITY	RECOVERY	FINAL DENS./COMPACT PROPS.
9202-01	DAC SYN 9225/1 (8h, 800°C, flowing Ar)	60.0 %			
9202-02	DAC NAT 9226/1 (8h, 800°C, flowing Ar)	58.75 %			
9202-03	WARREN/GE 300S, 101H-4 (8h, 800°C, flowing Ar)	56.60 %			
9202-04	WARREN/GE 300S, 927H-9 (70%) + 101H-4 (30%) (8h, 800°C, flowing Ar)	63.1 %			

NRL/DARPA DIAMOND POWDER COMPACTION EXPT. # 9

(SHOT # 9213, 12-CAPSULE SYSTEM, PW80 LENS, 1" PBX 9501, IMPACT VELOCITY = 1.835 km/s (center)

SAMPLE NUMBER	DIAMOND POWDER TYPE/MAKE & CONDITION	PACKING DENSITY	PLANARITY	RECOVERY	FINAL DENS./COMPACT PROPS.
9213-01	DAC SYN 9225(.4) + S90237(.6) (8h, 800°C, flowing Ar)	72.12%			86.92%
9213-02	DAC NAT 9226(.4) + N91168(.6) (8h, 800°C, flowing Ar)	73.63%			87.00%
9213-03	WARREN 101H-4(.4) + 927H-9(.6) (8h, 800°C, flowing Ar)	72.87%			92.90%
9213-04	DAC SYN 9225(.2) + S90237(.8) (8h, 800°C, flowing Ar)	75.87%			86.28%
9213-05	DAC NAT 9226(.2) + N91168(.8) (8h, 800°C, flowing Ar)	71.40%			86.02%
9213-06	WARREN 101H-4(.2) + 927H-9(.8) (8h, 800°C, flowing Ar)	75.22%			84.00%
9213-07	DAC SYN S90237 (8h, 800°C, flowing Ar)	64.77%			86.02%
9213-08	DAC NAT N91168 (8h, 800°C, flowing Ar)	67.91%			87.64%
9213-09	WARREN 927H-9 (8h, 800°C, flowing Ar)	67.90%		capsule blown	----- no recovery ----------
9213-10	DAC SYN S90237 + 10% Cu (8h, 800°C, flowing Ar)	65.33%			82.30%
9213-11	DAC NAT N91168 + 10% Cu (8h, 800°C, flowing Ar)	63.55%			-----
9213-12	Sodium Acetylide	59.45%			-----

NRL/DARPA DIAMOND POWDER COMPACTION EXPT. # 10

{SHOT # 9240, 12-CAPSULE SYSTEM, PW80 LENS, 1" PBX 9501, IMPACT VELOCITY = ????? km/s (center)

SAMPLE NUMBER	DIAMOND POWDER TYPE/MAKE & CONDITION	PACKING DENSITY	RECOVERY	FINAL DENS.	COMPACT PROPS.
9240-01	DHD-C (.5-1/10%,1-2/23%,16-20/67%) (8h, 800°C, flowing Ar)10%,1-2/23%,16-20/67%)	84.40%		87.93%	
9240-02	DHD-C (.5-1/10%,1-2/23%,16-20/67%) (8h, 800°C, flowing Ar)	84.57%		86.27%	
9240-03	DHD-F (0-.5/10%,.5-1/23%,8-12/67%) (8h, 800°C, flowing Ar)	72.97%		85.17%	
9240-04	DHD-F (0-.5/10%,.5-1/23%,8-12/67%) (8h, 800°C, flowing Ar)	80.52%		85.66%	
9240-05	WARREN 927H-9 (8h, 800°C, flowing Ar)	68.02%		87.31%	
9240-06	Allied Flourinated dia. (8h, 800°C, flowing Ar)	71.48%		89.56%	
9240-07	Allied Flourinated dia. (8h, 800°C, flowing Ar)	68.19%		NA	
9240-08	DHD-C(1-2/23%,16-20/67%)+Melamine/10% (8h, 800°C, flowing Ar)				
9240-09	DHD-F (.5-1/23%,8-12/67%) + Melamine/10% (8h, 800°C, flowing Ar)				
9240-10	Melamine/80% + Sig-Dia/20% (8-12) (8h, 800°C, flowing Ar)				
9240-11	Melamine/80% + Cu/20% (fine)				
9240-12	Sodium Acetylide + TiN				

APPENDIX - B

LISTING OF PUBLICATIONS

ON

DIAMOND POWDER COMPACTION EXPERIMENTS

Abstract Submitted
for the Shock Compression Topical Group Meeting of the
American Physical Society

at Colorado Springs, CO

Meeting Date: June 28 to July 2, 1993

Effect of Packing Density on Shock Consolidation of Diamond Powders. V. JOSHI, H.A. GREBE, EMRTC, New Mexico Tech, N.N. THADHANI, Georgia Institute of Technology, and Z. IQBAL, Allied-Signal Research and Technology. ---
Diamond powders of different types and particle size distributions were shock consolidated using a plate impact shock recovery system at 1.6 to 2.2 km/s. Single-piece diamond compacts (approximately 12 mm diameter and 1 mm thickness) with better than 90% relative densities were produced. A thin inter-particle boundary layer of a graphitic phase was identified in these compacts. While the effects of several different variables, e.g., powder pre-treatment, particle size and distribution, and impact conditions, were explored, it was established that the initial green powder compact density was the most important variable controlling the densification of diamond powders. In this paper, we will present results of some of the experiments and the role of initial green density in controlling the compact density and microstructure.

Abstract Submitted
for the TMS/ASM Meeting
at Pittsburg, PA

Meeting Date: October 17 - 21, 1993

DYNAMIC COMPACTION OF DIAMOND POWDERS FOR SUBSTRATE APPLICATIONS: V. Joshi, New Mexico Tech, Socorro, NM 87801; and N.N. Thadhani. Georgia Tech, Atlanta, GA 30332-0245.

Dynamic compaction of diamond powders was employed to fabricate 10 mm diameter by 1 mm thick wafers for possible substrate applications. Various models were used to predict the desired shock compaction conditions and starting powder/material characteristics. The experiments were performed at different compaction pressures, on diamond powders of different types, pre-treatments, particle sizes, distributions, and packing densities. The compacts were recovered as single piece macro-crack-free wafers with densities in the 90-95% TMD range. While evidence of interparticle melting, implying strong bonding, was clearly observed, formation of a graphitic phase was also revealed which resulted in significantly lower thermal conductivities. In this paper, we will review the consolidation models, and correlate their predictions to the experimental results, emphasizing the role of powder packing density on the characteristics of the recovered diamond compacts.